

---

# On Stability and Robustness of Diffusion Posterior Sampling for Bayesian Inverse Problems

---

Yiming Yang<sup>1</sup> Xiaoyuan Cheng<sup>2</sup> Yi He<sup>2</sup> Kaiyu Li<sup>1</sup> Wenxuan Yuan<sup>3</sup> Zhuo Sun<sup>†45</sup>

## Abstract

Diffusion models have recently emerged as powerful learned priors for Bayesian inverse problems (BIPs). Diffusion-based solvers rely on a presumed likelihood for the observations in BIPs to guide the generation process. However, the link between likelihood and recovery quality for BIPs is unclear in previous works. We bridge this gap by characterizing the posterior approximation error and proving the *stability* of the diffusion-based solvers. Meanwhile, an immediate result of our findings on stability demonstrates the lack of robustness in diffusion-based solvers, which remains unexplored. This can degrade performance when the presumed likelihood mismatches the unknown true data generation processes. To address this issue, we propose a simple yet effective solution, *robust diffusion posterior sampling*, which is provably *robust* and compatible with existing gradient-based posterior samplers. Empirical results on scientific inverse problems and natural image tasks validate the effectiveness and robustness of our method, showing consistent performance improvements under challenging likelihood misspecifications.

## 1. Introduction

The goal of Inverse Problems (IPs) is to recover the unknown variable  $\boldsymbol{x}$  given noisy measurements  $\boldsymbol{y} = \mathcal{F}(\boldsymbol{x}) + \epsilon$ . Because measurements are limited and noisy, IPs are often ill-posed (De Vito et al., 2005). IPs appear in various domains, such as medical imaging (Song et al., 2021c), geophysics (Sambridge & Mosegaard, 2002), and beyond.

<sup>1</sup>Department of Statistical Science, University College London, London, UK <sup>2</sup>Dynamic Systems Lab, University College London, London, UK <sup>3</sup>Department of Earth Science & Engineering, Imperial College London, London, UK <sup>4</sup>School of Statistics and Data Science, Shanghai University of Finance and Economics, Shanghai, P.R. China <sup>5</sup>Institute of Big Data Research, Shanghai University of Finance and Economics, Shanghai, P.R. China. <sup>†</sup>Correspondence to: Zhuo Sun <sunzhuo@mail.shufe.edu.cn>.

Bayesian inference mitigates the ill-posedness via a prior  $p(\boldsymbol{x})$  to regularize the solution based on prior knowledge. The likelihood  $p(\boldsymbol{y}|\boldsymbol{x})$  quantifies how well  $\mathcal{F}(\boldsymbol{x})$  explains the measurements  $\boldsymbol{y}$ . Applying Bayes' rule yields the posterior distribution  $p(\boldsymbol{x}|\boldsymbol{y})$ . This formulation is referred to as a Bayesian inverse problem (BIP), and the posterior is viewed as the solution (Sullivan, 2015).

Despite the simple formulation of BIPs, determining a suitable prior  $p(\boldsymbol{x})$  is both critical and challenging, particularly for high-dimensional complex data distributions. Apart from prior choices in existing works (Knapik et al., 2011; Wang et al., 2017; Hosseini & Nigam, 2017; Chung et al., 2023; Cardoso et al., 2024), probabilistic diffusion models (DMs) (Sohl-Dickstein et al., 2015; Song & Ermon, 2019; Ho et al., 2020; Song et al., 2021d) have emerged as powerful data-driven priors for solving inverse problems across various scenarios and applications (Zheng et al., 2025). DMs identify the target data distribution by reversing a forward diffusion process via a learned time-dependent score function  $\nabla_{\boldsymbol{x}_t} \log p(\boldsymbol{x}_t)$ , which progressively transports samples from Gaussian noise at time  $T$  to data samples from the target distribution  $p(\boldsymbol{x}_0)$  at time 0. Unlike standard BIPs, applying diffusion priors requires estimating intermediate posteriors  $p(\boldsymbol{x}_t|\boldsymbol{y})$  along the reverse diffusion process. These intermediate distributions are generally intractable. A widely adopted approach to address the intractability relies on *Tweedie's formula* (Efron, 2011) to obtain an estimate of the denoised conditional  $p(\boldsymbol{x}_0|\boldsymbol{x}_t)$ , effectively providing a point estimate (or a local Gaussian approximation) (Song et al., 2021a; Meng et al., 2021; Chung et al., 2023; Song et al., 2023a; Boys et al., 2024). This allows for a tractable likelihood approximation, which can then be combined with the diffusion prior to estimate intermediate posteriors along the reverse process and progressively solve the inverse problem; see Daras et al. (2024) for a review.

**On Stability for Diffusion-Based Solvers.** Although these methods have shown strong empirical performance for BIPs, the theoretical justification for their success is not yet fully established. Chung et al. (2023) and Song et al. (2023b) analyze the surrogate likelihood using the Tweedie approximation, but they still lack an investigation into the recovery quality for BIPs. We bridge this gap by: (1) proving

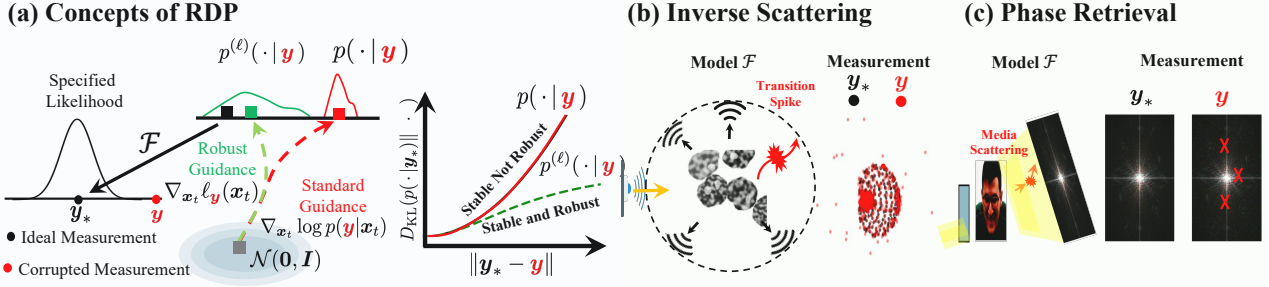


Figure 1. Overview. (a) Our proposed method achieves robust recovery under corruption. Visualization of the measurement model and data corruption, showing the sources of measurement corruption in (b) inverse scattering and (c) phase retrieval.

that the posterior induced by Diffusion Posterior Sampling (DPS) (Chung et al., 2023) is *stable*, and (2) quantifying the approximation error of the final posterior relative to the target distribution, showing that it scales with the magnitude of measurement noise.

**On Robustness for Diffusion-Based Solvers.** An immediate finding of our stability theorem is the lack of robustness of existing diffusion-based methods for BIPs. While robustness to likelihood misspecification is crucial, it remains largely underexplored. In BIPs, the likelihood  $p(\mathbf{y}|\mathbf{x})$  is determined by the measurement model  $\mathcal{F}$  and an assumed noise distribution  $\epsilon$  which can be misspecified in practice. For example, in optical tasks such as inverse scattering and phase retrieval, speckle noise or unexpected scattering from inhomogeneous media can produce heavy-tailed noise or outlier contamination, thereby violating the common Gaussian assumptions (see Figure 1(b)–(c)). In this setting, stable but non-robust diffusion-based solvers can drive the posterior far from the target one. One way to deal with likelihood misspecifications is to temper the likelihood with heuristic *temperatures* (Zhu et al., 2023; Chung et al., 2023; Song et al., 2023a;b; Wu et al., 2023; Cardoso et al., 2024), thereby globally down-weighting the likelihood term in the reverse diffusion processes. However, this global control is intended to stabilize the reverse sampling dynamics rather than explicitly mitigate the effect of likelihood misspecifications for BIPs.

To address likelihood misspecifications, we propose *robust diffusion posterior sampling*, a modular approach to robust BIP through the lens of generalized Bayesian inference (GBI). Our method acts as a plug-and-play module that can be integrated into existing gradient-based diffusion samplers. Figure 1(a) illustrates our proposed framework, designed to effectively mitigate the measurement corruptions visualized in panels (b) and (c). Experimental results confirm that our approach yields significant performance gains under likelihood misspecification while maintaining competitive performance in well-specified settings.

**Contributions.** We begin with our observations and theoretical results on the *stability of diffusion posterior sampling* methods for Bayesian inverse problems, which provide a formal justification for their effectiveness in solving Bayesian inverse problems. We characterize their vulnerability to likelihood misspecifications. Motivated by our analysis, we then introduce a general framework, *robust diffusion posterior sampling*, for robustness and propose a novel modular approach that seamlessly integrates with existing methods while providing theoretical guarantees of *robustness*. We empirically validate our observations and theory on the stability and robustness of diffusion-based solvers for BIPs and demonstrate the generality and robustness of the proposed method across a range of scientific inverse problems and image restoration tasks.

## 2. Background

In this section, we provide the necessary background knowledge about Bayesian inverse problems and diffusion-based solvers for these problems.

### 2.1. Bayesian Inverse Problems

A general inverse problem aims to recover the unknown variables  $\mathbf{x} \in \mathcal{X} \subset \mathbb{R}^{d_x}$  with compact  $\mathcal{X}$  from noisy observations  $\mathbf{y} \in \mathbb{R}^{d_y}$  given by:

$$\mathbf{y} = \mathcal{F}(\mathbf{x}) + \epsilon, \quad (1)$$

where  $\mathcal{F}: \mathcal{X} \rightarrow \mathbb{R}^{d_y}$  denotes the measurement model, and  $\epsilon \in \mathbb{R}^{d_y}$  denotes the additive measurement noise (Sullivan, 2015). Typically  $d_x \gg d_y$ , the inverse problem is underdetermined and requires regularization from prior knowledge.

Accordingly, the Bayesian inverse problem models the unknown  $\mathbf{x}$  as a random variable by specifying a prior  $p(\mathbf{x})$  on  $\mathcal{X}$ , and a likelihood  $p(\mathbf{y}|\mathbf{x})$  induced by (1) (Stuart, 2010; Sullivan, 2015). In this paper, we focus on the commonly used Gaussian likelihood, which factorizes across measurement components, i.e.,  $p(\mathbf{y}|\mathbf{x}) = \prod_{i=1}^{d_y} p(y_i|\mathbf{x})$ . Given an observation  $\mathbf{y}$ , Bayes' rule yields the posterior

$p(\mathbf{x}|\mathbf{y}) \propto p(\mathbf{y}|\mathbf{x})p(\mathbf{x})$ . However, traditional priors, such as the standard Gaussian, are often inadequate for representing the complex distributions of real-world data. Diffusion models, instead, offer a compelling choice for BIPs by learning expressive, data-driven priors (Song et al., 2021c;d).

## 2.2. Diffusion Models for Inverse Problems

Diffusion models provide a powerful framework for learning complex, high-dimensional distributions. In this work, we adopt the continuous-time Variance Preserving (VP) formulation. The forward process transforms a data sample  $\mathbf{x}_0$  into Gaussian noise over  $t \in [0, T]$ , governed by the stochastic differential equation (SDE)  $d\mathbf{x}_t = -\frac{1}{2}\beta(t)\mathbf{x}_t dt + \sqrt{\beta(t)}d\mathbf{w}$ , where  $\beta(t)$  is a predefined noise schedule and  $\mathbf{w}_t$  is a standard Wiener process. The key insight is that the forward process can be reversed in time using:

$$d\mathbf{x}_t = -\beta(t)\left[\frac{\mathbf{x}_t}{2} + \nabla_{\mathbf{x}_t} \log p(\mathbf{x}_t)\right]dt + \sqrt{\beta(t)}d\mathbf{w}_t. \quad (2)$$

The critical component required to solve the reverse SDE is the score function,  $\nabla_{\mathbf{x}_t} \log p_t(\mathbf{x}_t)$ , which is approximated by a time-dependent neural network  $\mathbf{s}_\theta(\mathbf{x}_t, t)$ . This network is trained via denoising score matching, minimizing the expected squared error between the predicted and true conditional scores. Once trained, the score network  $\mathbf{s}_\theta$  is used to generate samples by solving the reverse SDE, starting from  $\mathbf{x}_T \sim \mathcal{N}(\mathbf{0}, \mathbf{I})$ .

**Posterior Sampling with Diffusion Models** Solving a BIP requires sampling from the posterior  $p(\mathbf{x}_0|\mathbf{y})$ . This can be achieved by guiding the reverse SDE using the score of the posterior distribution at each time step  $\nabla_{\mathbf{x}_t} \log p_t(\mathbf{x}_t|\mathbf{y})$ . Using Bayes' theorem, this posterior score can be decomposed into a prior and a likelihood:

$$\nabla_{\mathbf{x}_t} \log p_t(\mathbf{x}_t|\mathbf{y}) = \underbrace{\nabla_{\mathbf{x}_t} \log p_t(\mathbf{x}_t)}_{\text{Prior Score}} + \underbrace{\nabla_{\mathbf{x}_t} \log p(\mathbf{y}|\mathbf{x}_t)}_{\text{Likelihood Score}}.$$

The prior score is readily available from the pre-trained score network, i.e.,  $\mathbf{s}_\theta(\mathbf{x}_t, t)$ . The likelihood term is challenging to derive, as the time-dependent likelihood function  $p(\mathbf{y}|\mathbf{x}_t) = \int p(\mathbf{y}|\mathbf{x}_0)p(\mathbf{x}_0|\mathbf{x}_t) d\mathbf{x}_0 = \mathbb{E}[p(\mathbf{y}|\mathbf{x}_0)]$  is not tractable in general.

An efficient strategy is to approximate the intractable likelihood  $p(\mathbf{y}|\mathbf{x}_t)$  with a surrogate  $p(\mathbf{y}|\mathbf{x}_t) \approx \tilde{p}(\mathbf{y}|\hat{\mathbf{x}}_0(\mathbf{x}_t))$ , which is the likelihood evaluated at  $\hat{\mathbf{x}}_0(\mathbf{x}_t)$ , the estimate of  $\mathbf{x}_0$  at step  $t$  from the diffusion model (Stein, 1981; Efron, 2011; Graikos et al., 2022; Chung et al., 2023). We refer to this surrogate likelihood as *DPS* likelihood. While the DPS approximation has proven effective for well-specified likelihood models (Song et al., 2021a; Ho et al., 2022; Wu et al., 2023; Song et al., 2023b), its robustness to likelihood misspecifications remains a concern. Likelihood misspecifications can arise from the misspecification of the noise

distribution or from the presence of a contaminated subset of observations generated under a different data-generating mechanism. In this work, we investigate the impact of such misspecifications and aim to answer the following questions:

*Is diffusion posterior sampling robust to likelihood misspecifications? If not, can we propose a solution that guarantees robust recovery without losing the effectiveness?*

## 3. Method

This section begins by establishing the stable properties of the standard diffusion sampler, which also shows its vulnerability to likelihood misspecification. We then formulate a robust strategy with theoretical guarantees and detail its practical implementation for general BIPs with diffusion solvers. Finally, we analyze how our robust approach performs in well-specified settings.

We address the setting in which observations may be contaminated, for example, by measurement errors or outliers:  $\mathbf{y} = \mathbf{y}_* + \epsilon$ . This contains both nominal noise and sparse outliers. Our goal is to sample from a robust posterior that approximates the target distribution  $p(\cdot|\mathbf{y}_*)$  despite the presence of outliers. To proceed, we assume the following conditions hold throughout the paper.

**Assumption 3.1** (Measurement Model Regularity). The measurement model  $\mathcal{F}$  is twice differentiable,  $\mathcal{F} \in C^2$ .

**Assumption 3.2** (Score Network Regularity). For any time  $t$ ,  $\mathbf{s}_\theta(\mathbf{x}, t)$  is Lipschitz continuous in  $\mathbf{x}$ .

**Assumption 3.3** (Score Approximation Error). For any time  $t$ ,  $\mathbb{E}[\|\nabla_{\mathbf{x}_t} \log p_t(\mathbf{x}) - \mathbf{s}_\theta(\mathbf{x}, t)\|_2^2] \leq \epsilon_s(t)^2$ .

Assumption 3.1 is standard in BIP and is automatically satisfied by linear measurement models. Assumptions 3.2 and 3.3 are standard in the context of diffusion models (Song et al., 2021b;d).

### 3.1. Stability and Robustness of Diffusion Posterior

Following the likelihood approximation in Section 2.2, the likelihood score is evaluated as  $\nabla_{\mathbf{x}_t} \log p(\mathbf{y}|\mathbf{x}_t) \approx \nabla_{\mathbf{x}_t} \log \tilde{p}(\mathbf{y}|\hat{\mathbf{x}}_0(\mathbf{x}_t))$ . The  $\hat{\mathbf{x}}_0(\mathbf{x}_t)$  is the denoised estimate of the clean data given  $\mathbf{x}_t$ , defined by

$$\hat{\mathbf{x}}_0(\mathbf{x}_t) = \mathbb{E}(\mathbf{x}_0|\mathbf{x}_t) \approx \frac{1}{\sqrt{\alpha(t)}}(\mathbf{x}_t + (1 - \alpha(t))\mathbf{s}_\theta(\mathbf{x}_t, t)),$$

where  $\alpha(t) = \exp(-\int_0^t \beta(\tau)d\tau)$ . Then, one can perform posterior sampling by solving the reverse SDE as in Equation 2, substituting the unconditional score  $\nabla_{\mathbf{x}_t} \log p(\mathbf{x}_t)$  with the approximated posterior score  $\nabla_{\mathbf{x}_t} \log \tilde{p}(\mathbf{x}_t|\mathbf{y}) = \mathbf{s}_\theta(\mathbf{x}_t, t) + \nabla_{\mathbf{x}_t} \log \tilde{p}(\mathbf{y}|\hat{\mathbf{x}}_0(\mathbf{x}_t))$ . While Chung et al. (2023) and Song et al. (2023b) analyze the DPS likelihood error, their link to recovery quality is indirect. The following

Theorem 3.4 bridges this gap by (1) establishing the stability of the DPS solver and (2) quantifying the posterior approximation error.

**Theorem 3.4.** *Consider the posterior  $\tilde{p}(\cdot|\mathbf{y})$  induced by the DPS solver under Assumptions 3.1–3.3 with a specified Gaussian likelihood  $\mathbf{y}|\mathbf{x} \sim \mathcal{N}(\mathcal{F}(\mathbf{x}), \sigma_y^2 \mathbf{I})$ . Then, we have:*

**(Solver Stability)** *The posterior mapping  $\mathbf{y} \mapsto \tilde{p}(\cdot|\mathbf{y})$  is Lipschitz continuous with respect to the measurement  $\mathbf{y}$ . Specifically, for any  $\mathbf{y}, \mathbf{y}' \in \mathbb{R}^{d_y}$ , there exists a finite constant  $C_{stable}$  such that:*

$$D_{KL}(\tilde{p}(\cdot|\mathbf{y})||\tilde{p}(\cdot|\mathbf{y}')) \leq C_{stable} \|\mathbf{y} - \mathbf{y}'\|_2^2. \quad (3)$$

**(Total Error)** *Let  $p(\cdot|\mathbf{y}_*)$  denote the target posterior governed by the exact score and likelihood, conditioned on the noiseless measurement  $\mathbf{y}_* = \mathcal{F}(\mathbf{x})$ . The KL divergence with respect to the target posterior satisfies:*

$$D_{KL}(p(\cdot|\mathbf{y}_*)||\tilde{p}(\cdot|\mathbf{y})) \leq C_\theta + \underbrace{C_{stable} \|\mathbf{y}_* - \mathbf{y}\|_2^2}_{\text{Stability Error}}$$

where  $C_\theta$  is from the cumulative score estimation error.

The detailed proof is provided in Appendix D. Theorem 3.4 indicates that the approximation error is bounded by a term quadratic in the measurement noise magnitude  $\|\mathbf{y}_* - \mathbf{y}\|_2$ . This result confirms the stability of the diffusion prior under the DPS likelihood approximation, validating its effectiveness for moderate noise levels (Chung et al., 2023) that align with the assumed Gaussian likelihood model. However, the error is radially unbounded and scales rapidly as the noise magnitude increases. This lack of robustness in the DPS solver motivates our robust solution.

Before proceeding, we first give the definition of robustness by quantifying how the posterior distribution changes in response to measurement perturbations. Following Altamirano et al. (2023); Duran-Martin et al. (2024), the posterior influence function (PIF) is defined as the KL divergence such that

$$\text{PIF}_{\mathbf{y}_*}(\mathbf{y}) := D_{KL}(p(\mathbf{x}|\mathbf{y}_*)||p(\mathbf{x}|\mathbf{y})).$$

The posterior is called *robust* if the PIF is uniformly bounded, i.e.,  $\sup_{\mathbf{y} \in \mathbb{R}^{d_y}} |\text{PIF}_{\mathbf{y}_*}(\mathbf{y})| < \infty$ .

### 3.2. Robust Diffusion Posterior

To address this issue, we consider generalized Bayes (GB) (Sullivan, 2015) in this work. GB considers alternative differentiable loss functions  $\ell_{\mathbf{y}} : \mathcal{X} \rightarrow \mathbb{R}$  in place of the negative log-likelihood in Bayes' rule. The subscript  $\mathbf{y}$  denotes the dependence on the observation  $\mathbf{y}$ . The loss  $\ell_{\mathbf{y}}$  can be flexibly specified under mild regularity conditions;

see Section 6.3 of Sullivan (2015). This yields the generalized posterior (Matsubara et al., 2022; Wild et al., 2023; Altamirano et al., 2023) in the following form,

$$p^{(\ell)}(\mathbf{x}|\mathbf{y}) \propto p(\mathbf{x}) \exp\{-\tau \ell_{\mathbf{y}}(\mathbf{x})\},$$

where  $\tau > 0$  is a temperature parameter that controls the influence of the loss relative to the prior. Many choices of  $\ell$  (e.g., density-power) are well established and show improved performance under likelihood misspecification (Huber, 2011; Song & Huang, 2024).

However, these works typically study robustness under contamination models formed as a mixture of the empirical distribution of the true data-generating distribution and a Dirac measure located away from it. Such settings assume multiple observations, with robustness defined in terms of the contamination of only part of the data. Differently, BIPs focus on the posterior conditioning on a *single* (high-dimensional) measurement, where contamination is structured and often occurs at the level of coordinates or components, e.g., pixel-wise for images (e.g., pixel-wise outliers; see Figure 1 (b)-(c)), thereby making standard GB constructions nontrivial to apply in this setting.

To gain robustness in BIPs, we therefore choose  $\ell_{\mathbf{y}}$  to be an adaptively weighted data misfit and refer to the resulting method as the Robust Diffusion Posterior (RDP). We design the RDP by guiding the reverse diffusion with a robust weighted likelihood. Practically, we follow the additive form of likelihood as discussed in Section 2.1 and retain the DPS approximation  $\tilde{p}(\mathbf{y}|\mathbf{x}_t) \approx p(\mathbf{y}|\mathbf{x}_t)$  by evaluating the likelihood at the denoised estimate of clean data,  $\hat{\mathbf{x}}_0(\mathbf{x}_t)$ . RDP achieves robustness by transforming the DPS guidance term into a component-wise weighted objective. At diffusion time  $t$ , we define the loss function  $\ell_{\mathbf{y}}(\mathbf{x}_t) = -\sum_{i=1}^{d_y} w(r_{t,i}) \log \tilde{p}(y_i|\hat{\mathbf{x}}_{0|t})$ , where  $r_{t,i} = y_i - \hat{y}_{t,i}$  and  $\hat{y}_{t,i} := [\mathcal{F}(\hat{\mathbf{x}}_{0|t})]_i$  denote the fitting residual and the predicted measurements, respectively. The loss function induces the robust diffusion posterior  $p_t^{(\ell)}(\mathbf{x}_t|\mathbf{y}) \propto p(\mathbf{x}_t) \exp\{-\tau \ell_{\mathbf{y}}(\hat{\mathbf{x}}_{0|t})\}$  at time  $t$ . The term  $w : \mathbb{R} \rightarrow \mathbb{R}$  is a component-wise adaptive weight function. This weighting mechanism acts as a robust filter: for small residuals,  $w_i \approx 1$ , which recovers standard likelihood; conversely, large residuals are down-weighted to limit the influence of outliers.

We now provide a sufficient condition for the design of the weighting function  $w$  that guaranties robustness of the diffusion posterior, formalized in the following result:

**Theorem 3.5.** *Consider the robust diffusion posterior with the score  $\nabla_{\mathbf{x}_t} \log p^{(\ell)}(\mathbf{x}_t|\mathbf{y}) = \mathbf{s}_\theta(\mathbf{x}_t, t) - \nabla_{\mathbf{x}_t} \ell_{\mathbf{y}}(\mathbf{x}_t)$ . Let the guidance loss be defined by  $\ell_{\mathbf{y}}(\mathbf{x}_t) = -\sum_{i=1}^{d_y} w(r_i) \log p(y_i|\hat{\mathbf{x}}_{0|t})$ , where  $r_i = y_i - [\mathcal{F}(\hat{\mathbf{x}}_{0|t})]_i$  denotes the residual and  $w(\cdot)$  is a differentiable weighting function. Suppose that Assumption 3.1 and Assumption 3.2*

hold. If the weighting function  $w$  satisfies the following conditions for any  $r \in \mathbb{R}$ :

$$|r w(r)| < \infty \quad \text{and} \quad |r^2 w'(r)| < \infty, \quad (4)$$

where  $w'$  is the gradient of  $w$  w.r.t.  $r$ . Then, for  $\mathbf{x} \in \mathcal{X}$ , the posterior KL divergence is uniformly bounded:

$$\sup_{\mathbf{y} \in \mathbb{R}^{d_y}} D_{\text{KL}}(p^{(\ell)}(\cdot | \mathbf{y}_*) | p^{(\ell)}(\cdot | \mathbf{y})) \leq C,$$

where  $C$  is a finite constant independent of the measurement  $\mathbf{y}$ . Equivalently, the posterior  $p_t^{(\ell)}$  is robust, satisfying  $\sup_{\mathbf{y} \in \mathbb{R}^{d_y}} |PIF_{\mathbf{y}_*}(\mathbf{y})| < \infty$ .

The proof is provided in Appendix D.3. This result stands in contrast to the standard DPS solver, where the PIF is unbounded. In contrast, the proposed robust conditions limit the influence of severe noise misspecification in measurement  $\mathbf{y}$ , thereby mitigating the risk of destabilizing the generation process.

*Remark 3.6 (Choice of  $w$ ).* The inverse multi-quadratic (IMQ) weighting function, defined as  $w(r) = (1 + r^2/c^2)^{-1/2}$ , satisfies the conditions established in Theorem 3.5. Consequently, the resulting diffusion posterior is outlier-robust. In this work, we adopt  $w$  in the IMQ form  $w(r_i) = (1 + r_i^2/c^2)^{-1/2}$  for  $i = 1, \dots, d_y$ , where  $c > 0$  is a soft threshold: a larger value of  $c$  keeps weights closer to uniform, while a smaller value strongly down-weights large residuals. See Appendix E.2 for additional discussion on alternative weight functions.

Algorithm 1 presents RDP instantiated within the DPS sampler, which provides a realization aligned with the analysis in this paper. More broadly, RDP is a modular plug-in that can be incorporated into a broad class of plug-and-play diffusion-based approaches. We outline a general version in Appendix E.1 Algorithm 2 and provide associated experimental results in Section 4.

---

#### Algorithm 1 Robust Diffusion Posterior Sampling

---

**Require:** observation  $\mathbf{y}$ , score network  $\mathbf{s}_\theta$ , noise schedule  $\{\beta_t\}_{t=0}^T$ , weight function  $w(\cdot)$ , temperature  $\{\tau_t\}_{t=0}^T$

- 1: Initialize  $\mathbf{x}_T \sim \mathcal{N}(\mathbf{0}, \mathbf{I})$
  - 2: **for**  $t = T, \dots, 1$  **do**
  - 3:    $\alpha_t = 1 - \beta_t$ ,    $\bar{\alpha}_t = \prod_{i=1}^t \alpha_i$
  - 4:    $\hat{\mathbf{x}}_{0|t} = \frac{1}{\sqrt{\bar{\alpha}_t}}(\mathbf{x}_t + (1 - \bar{\alpha}_t)\mathbf{s}_\theta(\mathbf{x}_t, t))$
  - 5:    $\mathbf{r} = \mathbf{y} - \hat{\mathbf{y}}$  with  $\hat{\mathbf{y}} = \mathcal{F}(\hat{\mathbf{x}}_{0|t})$
  - 6:    $\mathbf{W} = (w(r_1), \dots, w(r_m))$
  - 7:    $\ell_{\mathbf{y}}(\mathbf{x}_t) = \mathbf{W}^\top \log p(\mathbf{y} | \hat{\mathbf{x}}_{0|t}(\mathbf{x}_t))$
  - 8:    $\hat{\mathbf{s}} = \mathbf{s}_\theta(\mathbf{x}_t, t) - \tau_t \nabla_{\mathbf{x}_t} \ell_{\mathbf{y}}(\mathbf{x}_t)$
  - 9:    $\mathbf{z} \sim \mathcal{N}(\mathbf{0}, \mathbf{I})$  if  $t > 1$  else  $\mathbf{0}$
  - 10:    $\mathbf{x}_{t-1} = \mathbf{x}_t + \beta_t (\frac{1}{2} \mathbf{x}_t + \hat{\mathbf{s}})$
  - 11: **end for**
- 

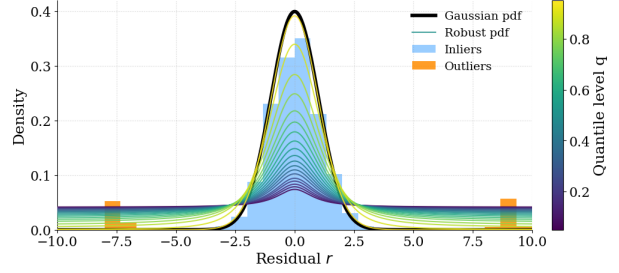


Figure 2. Histogram of residuals and outliers compared against Gaussian (black) and robust pdfs (colored) across quantiles  $q$ .

**Performance given Nominal Measurements.** So far, we have established the robustness of RDP in worst-case scenarios. A natural follow-up question is:

*How does RDP perform under nominal measurements?*

To answer this question, we analyze the KL divergence between (i) the target diffusion posterior  $p_t$  induced by a Gaussian likelihood and (ii) the RDP posterior  $p_t^{(\ell)}$  with the IMQ weighting function:

**Corollary 3.7.** *Suppose that the assumptions and conditions of Theorem 3.5 hold. Then, for any  $\mathbf{x} \in \mathcal{X}$ , the posterior KL divergence:*

$$D_{\text{KL}}(p(\cdot | \mathbf{y}_*) | p^{(\ell)}(\cdot | \mathbf{y}_*)) \leq C_\theta + C_\ell,$$

where  $C_\theta$  is the same as in theorem 3.4 and  $C_\ell = O(c^{-4})$ .

The proof is provided in Appendix D.3. The term  $C_\ell$  represents the irreducible bias arising from using robust guidance when the true measurement model  $\mathbf{y} | \mathbf{x}$  is actually well-specified. This is analogous to the discussion in standard Bayesian problems (Knoblauch et al., 2022). Specifically, for the IMQ weighting function, we find that  $C_\ell = O(c^{-4})$ . A larger  $c$  favors high fidelity for clean data (low bias), while a smaller  $c$  provides stronger suppression of large fitting residuals (high robustness).

*Remark 3.8.* In practice, we adopt an adaptive schedule for the parameter  $c$ . Rather than relying on a fixed  $c$ , we dynamically calibrate  $c_t$  at each timestep  $t$  based on the statistics of the current fitting residuals. Specifically, we set  $c_t$  based on the  $q$ -th quantile of the absolute residuals:  $c_t = \text{Quantile}_q(|\mathbf{r}_t|)$ , where  $q \in (0, 1]$  and  $\mathbf{r}_t = (r_{t,1}, \dots, r_{t,d_y})$ . By setting the parameter  $c$  at the  $q$ -th quantile, the posterior update is primarily driven by the  $q\%$  of measurements with the smallest errors, while limiting the impact of the remaining  $(1 - q)\%$ ; see Figure 2. In the reverse generative process, the magnitude of fitting residuals  $\mathbf{r}_t$  tends to decrease as  $t \rightarrow 0$ . Unlike a fixed parameter, this adaptive schedule accounts for these dynamic changes over time.

Table 1. Quantitative results on *Inverse Scattering* are reported as PSNR, SSIM, and NMAE (mean  $\pm$  std) over 100 test samples. Results on *FFHQ-Inpaint*, *-Deblur*, and *-Phase Retrieval*, reported in LPIPS ( $\downarrow$ ), VIFL ( $\downarrow$ ) as mean  $\pm$  std, and FID ( $\downarrow$ ) on 500 test images.

Task	Method	Well-specification (Gaussian)			Noise Misspecification (Student-T)			Contamination of Outliers			
		PSNR( $\uparrow$ )	SSIM( $\uparrow$ )	NMAE( $\downarrow$ )	PSNR( $\uparrow$ )	SSIM( $\uparrow$ )	NMAE( $\downarrow$ )	PSNR( $\uparrow$ )	SSIM( $\uparrow$ )	NMAE( $\downarrow$ )	
Inverse Scattering	DPS	<b>26.26 <math>\pm</math> 2.83</b>	0.86 $\pm$ 0.02	0.16 $\pm$ 0.02	21.53 $\pm$ 2.93	0.78 $\pm$ 0.06	0.25 $\pm$ 0.05	19.37 $\pm$ 3.44	0.71 $\pm$ 0.10	0.33 $\pm$ 0.05	
	LGD	24.16 $\pm$ 2.95	0.76 $\pm$ 0.20	0.18 $\pm$ 0.09	18.80 $\pm$ 2.54	0.62 $\pm$ 0.07	0.34 $\pm$ 0.10	17.81 $\pm$ 2.89	0.53 $\pm$ 0.12	0.36 $\pm$ 0.05	
	$\Pi$ GDM	24.23 $\pm$ 2.26	0.81 $\pm$ 0.13	0.18 $\pm$ 0.07	21.17 $\pm$ 3.15	0.69 $\pm$ 0.05	0.24 $\pm$ 0.05	15.14 $\pm$ 3.88	0.64 $\pm$ 0.15	0.37 $\pm$ 0.06	
	PnPDM	25.77 $\pm$ 2.75	<b>0.87 <math>\pm</math> 0.04</b>	<b>0.14 <math>\pm</math> 0.03</b>	20.38 $\pm$ 4.14	0.73 $\pm$ 0.12	0.27 $\pm$ 0.21	15.33 $\pm$ 3.23	0.73 $\pm$ 0.12	0.30 $\pm$ 0.03	
	RDP-DPS	26.01 $\pm$ 2.72	0.86 $\pm$ 0.02	0.15 $\pm$ 0.01	<b>23.84 <math>\pm</math> 2.59</b>	<b>0.82 <math>\pm</math> 0.03</b>	<b>0.19 <math>\pm</math> 0.04</b>	<b>25.24 <math>\pm</math> 2.74</b>	<b>0.83 <math>\pm</math> 0.02</b>	<b>0.15 <math>\pm</math> 0.02</b>	
	RDP-LGD	24.88 $\pm$ 2.17	0.81 $\pm$ 0.06	0.18 $\pm$ 0.03	21.83 $\pm$ 2.25	0.79 $\pm$ 0.05	0.23 $\pm$ 0.04	25.02 $\pm$ 2.23	0.70 $\pm$ 0.06	0.21 $\pm$ 0.03	
	RDP- $\Pi$ GDM	23.67 $\pm$ 2.15	0.79 $\pm$ 0.07	0.17 $\pm$ 0.04	22.23 $\pm$ 2.18	0.72 $\pm$ 0.02	0.19 $\pm$ 0.03	22.49 $\pm$ 2.36	0.78 $\pm$ 0.05	0.21 $\pm$ 0.04	
	RDP-PnPDM	23.94 $\pm$ 2.05	0.86 $\pm$ 0.04	0.16 $\pm$ 0.02	22.15 $\pm$ 3.11	0.79 $\pm$ 0.06	0.21 $\pm$ 0.02	23.45 $\pm$ 2.95	0.81 $\pm$ 0.07	0.16 $\pm$ 0.03	
			LPIPS( $\downarrow$ )	VIFL( $\downarrow$ )	FID( $\downarrow$ )	LPIPS( $\downarrow$ )	VIFL( $\downarrow$ )	FID( $\downarrow$ )	LPIPS( $\downarrow$ )	VIFL( $\downarrow$ )	FID( $\downarrow$ )
	Inpaint	DPS	0.19 $\pm$ 0.04	0.62 $\pm$ 0.04	27.19	0.25 $\pm$ 0.06	0.70 $\pm$ 0.04	30.21	0.37 $\pm$ 0.06	0.89 $\pm$ 0.04	41.27
LGD		0.21 $\pm$ 0.03	0.68 $\pm$ 0.04	28.04	0.24 $\pm$ 0.04	0.75 $\pm$ 0.05	31.79	0.34 $\pm$ 0.06	0.85 $\pm$ 0.03	37.93	
$\Pi$ GDM		0.21 $\pm$ 0.05	0.63 $\pm$ 0.03	28.72	0.29 $\pm$ 0.03	0.77 $\pm$ 0.04	40.28	0.38 $\pm$ 0.06	0.84 $\pm$ 0.04	47.93	
PnPDM		<b>0.19 <math>\pm</math> 0.03</b>	<b>0.61 <math>\pm</math> 0.04</b>	<b>27.17</b>	0.25 $\pm$ 0.04	0.73 $\pm$ 0.04	31.29	0.36 $\pm$ 0.04	0.80 $\pm$ 0.05	47.28	
RDP-DPS		0.20 $\pm$ 0.04	0.62 $\pm$ 0.05	27.62	<b>0.21 <math>\pm</math> 0.04</b>	<b>0.66 <math>\pm</math> 0.04</b>	<b>28.03</b>	<b>0.24 <math>\pm</math> 0.04</b>	<b>0.70 <math>\pm</math> 0.03</b>	<b>29.95</b>	
RDP-LGD		0.22 $\pm$ 0.04	0.69 $\pm$ 0.04	28.60	0.23 $\pm$ 0.05	0.72 $\pm$ 0.03	29.52	0.25 $\pm$ 0.05	0.77 $\pm$ 0.04	30.06	
RDP- $\Pi$ GDM		0.20 $\pm$ 0.04	0.63 $\pm$ 0.03	29.15	0.24 $\pm$ 0.04	0.70 $\pm$ 0.04	28.19	0.25 $\pm$ 0.04	0.74 $\pm$ 0.05	30.27	
RDP-PnPDM		0.20 $\pm$ 0.04	0.65 $\pm$ 0.03	27.66	0.23 $\pm$ 0.04	0.71 $\pm$ 0.03	29.35	<b>0.24 <math>\pm</math> 0.04</b>	0.73 $\pm$ 0.04	30.20	
Deblur		DPS	0.17 $\pm$ 0.04	0.61 $\pm$ 0.05	26.98	0.20 $\pm$ 0.04	0.69 $\pm$ 0.04	29.35	0.32 $\pm$ 0.07	0.83 $\pm$ 0.07	39.82
		LGD	<b>0.13 <math>\pm</math> 0.03</b>	<b>0.58 <math>\pm</math> 0.04</b>	<b>22.36</b>	0.17 $\pm$ 0.04	0.67 $\pm$ 0.05	22.84	0.33 $\pm$ 0.09	0.79 $\pm$ 0.08	33.39
	$\Pi$ GDM	0.19 $\pm$ 0.08	0.62 $\pm$ 0.06	30.77	0.29 $\pm$ 0.11	0.71 $\pm$ 0.14	55.76	0.39 $\pm$ 0.15	0.90 $\pm$ 0.18	59.32	
	PnPDM	0.14 $\pm$ 0.04	0.59 $\pm$ 0.04	24.11	0.21 $\pm$ 0.05	0.70 $\pm$ 0.04	35.18	0.35 $\pm$ 0.04	0.84 $\pm$ 0.04	42.54	
	RDP-DPS	0.17 $\pm$ 0.04	0.62 $\pm$ 0.04	26.39	0.18 $\pm$ 0.04	0.65 $\pm$ 0.03	27.81	0.25 $\pm$ 0.06	0.75 $\pm$ 0.03	30.60	
	RDP-LGD	0.14 $\pm$ 0.05	0.61 $\pm$ 0.05	21.84	<b>0.14 <math>\pm</math> 0.03</b>	<b>0.63 <math>\pm</math> 0.04</b>	<b>22.71</b>	<b>0.22 <math>\pm</math> 0.05</b>	<b>0.70 <math>\pm</math> 0.04</b>	<b>28.55</b>	
	RDP- $\Pi$ GDM	0.20 $\pm$ 0.06	0.63 $\pm$ 0.05	30.86	0.21 $\pm$ 0.04	0.69 $\pm$ 0.05	33.94	0.31 $\pm$ 0.06	0.83 $\pm$ 0.07	38.84	
	RDP-PnPDM	0.16 $\pm$ 0.04	0.61 $\pm$ 0.03	25.73	0.18 $\pm$ 0.04	0.65 $\pm$ 0.04	27.69	0.25 $\pm$ 0.05	0.77 $\pm$ 0.04	33.92	
	Phase Retrieval	DPS	0.45 $\pm$ 0.17	0.76 $\pm$ 0.03	62.16	0.52 $\pm$ 0.18	0.85 $\pm$ 0.03	76.01	0.64 $\pm$ 0.22	0.96 $\pm$ 0.02	118.59
		LGD	0.43 $\pm$ 0.19	0.79 $\pm$ 0.04	64.86	0.55 $\pm$ 0.21	0.89 $\pm$ 0.04	95.42	0.60 $\pm$ 0.17	0.95 $\pm$ 0.05	140.72
PnPDM		<b>0.38 <math>\pm</math> 0.13</b>	<b>0.72 <math>\pm</math> 0.04</b>	<b>57.04</b>	0.49 $\pm$ 0.17	0.82 $\pm$ 0.03	74.38	0.60 $\pm$ 0.20	0.93 $\pm$ 0.04	113.82	
RDP-DPS		0.43 $\pm$ 0.13	0.76 $\pm$ 0.02	61.29	0.49 $\pm$ 0.12	0.81 $\pm$ 0.02	73.51	<b>0.51 <math>\pm</math> 0.14</b>	<b>0.82 <math>\pm</math> 0.04</b>	<b>75.07</b>	
RDP-LGD		0.43 $\pm$ 0.16	0.79 $\pm$ 0.04	63.37	0.51 $\pm$ 0.14	0.83 $\pm$ 0.05	76.28	0.54 $\pm$ 0.09	0.88 $\pm$ 0.03	84.27	
RDP-PnPDM		0.40 $\pm$ 0.12	0.74 $\pm$ 0.02	58.93	<b>0.47 <math>\pm</math> 0.13</b>	<b>0.77 <math>\pm</math> 0.31</b>	<b>63.93</b>	0.52 $\pm$ 0.16	<b>0.82 <math>\pm</math> 0.04</b>	75.31	

## 4. Experiments

In this section, we validate the effectiveness and robustness of the proposed RDP method. We demonstrate RDP’s generality by integrating it with four representative diffusion-based inverse solvers, including DPS (Chung et al., 2023), LGD (Song et al., 2023b),  $\Pi$ GDM (Song et al., 2023a), and PnPDM (Wu et al., 2024)<sup>1</sup>. See Algorithm 1 and Algorithm 2 for the pseudo-code of our algorithms. For fair comparisons, all methods are evaluated using the same pre-trained score/denoising models and sampling schedule. We refer to the RDP version of method X as RDP-X; for example, RDP-DPS denotes DPS with RDP guidance. Implementation code is available in the supplementary material.

### 4.1. Experimental Settings

**Tasks.** We conduct comprehensive experiments on a diverse range of scientific inverse problems and natural

image restorations using the open-source benchmark *InverseBench*<sup>2</sup> (Zheng et al., 2025). The tasks include: (1) inverse scattering (IS), (2) image inpainting, (3) deblurring, and (4) phase retrieval on the FFHQ-256 dataset (FFHQ-D/PR), covering both linear and nonlinear tasks. In practice, these problems often suffer from likelihood misspecification; for example, phase retrieval can be affected by unexpected scattering from inhomogeneous media and other unmodeled physical corruptions. Such effects can introduce heavy-tailed noise or outlier contamination that violates Gaussian assumptions, making these tasks well suited for evaluating robust reconstruction.

**Experimental Design.** A central focus of our evaluation is the performance regarding the mismatched noise distribution. We introduce two different schemes applied in the observation domain: (1) *Heavy-tailed noise*: i.i.d. noises from the Student-t distribution for evaluating the performance under the misspecification of the noise distribution; and (2) *Sparse impulsive outlier*: a fraction of components/pixels corrupted by large-magnitude perturbations for evaluating

<sup>2</sup><https://github.com/devzhk/InverseBench>

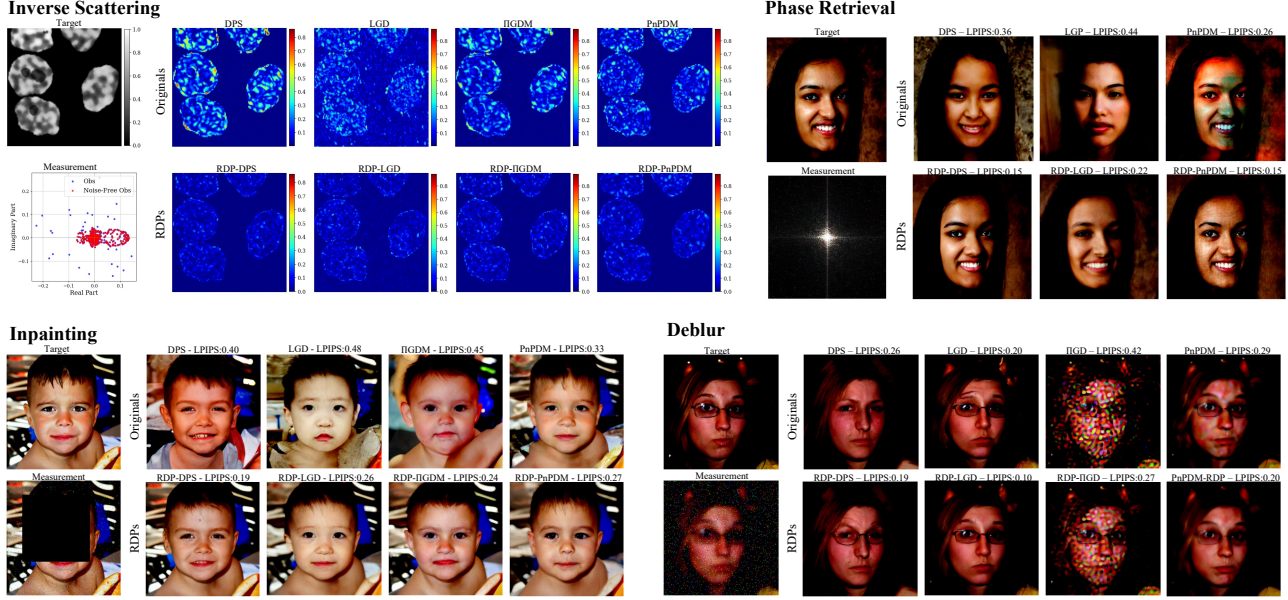


Figure 3. Qualitative results on all outlier-corrupted tasks: (a) Inverse Scattering, (b) Phase Retrieval, (c) Deblurring, and (d) Inpainting. In each panel, the leftmost column shows the ground truth and the measurements. The remaining columns compare the originals (top row) with their robust versions (bottom row); we report reconstruction absolute errors in (a) and reconstructed samples in (b)–(d).

the performance under outlier contamination. Additionally, to evaluate our approaches under nominal observations, we also report results with the conventional i.i.d. Gaussian noise distribution. See Section F.2 for specific settings for each experiment.

**Evaluation Metric.** For the IS problem, we quantify the reconstruction quality using peak signal-to-noise ratio (PSNR) and structural similarity (SSIM). To reflect robustness under heavy-tailed noise and impulsive outliers, we also report the normalized mean absolute error (NMAE) as a robust metric, which complements PSNR/SSIM in such settings. For the two natural image tasks, we use standard perceptual quality metrics for natural images: learned perceptual image patch similarity (LPIPS), visual information fidelity loss (VIFL), and Fréchet Inception Distance (FID) using the pre-trained InceptionV3 (Szegedy et al., 2016).

#### 4.2. Result Analysis

In this section, we now answer the following questions with findings from our experiments.

(1) *Does a diffusion-model prior lead to posterior stability and convergence when measurements match the presumed likelihood model?*

The answer is affirmative. Quantitatively, it is evidenced by the first columns under the Gaussian noise setting in Table 1. In cases where the Gaussian likelihood is well-

specified, we report competitive performance benchmarks across standard methods such as DPS, LGD, IIGDM, and PnPDM, indicating that the approximation supports stable convergence. This result is also supported qualitatively in Figure 4 (left columns of each sub figure), where density contours of the first two latent dimensions for samples and targets show a strong overlap. Furthermore, we observe that incorporating our proposed robust module preserves this stability while maintaining performance competitive with the original approaches across all tasks.

(2) *Can diffusion samplers fail under likelihood misspecification, and does RDP effectively mitigate this failure?*

Yes, to both questions.

(DEGRADATION OF ORIGINAL APPROACH.) Original approaches typically rely on a presumed Gaussian likelihood and have been shown to suffer from large degradation under likelihood misspecification: (i) misspecification of the noise distribution; (ii) contamination by outliers. For inverse scattering performance at the top of Table 1, we observe that baseline methods show substantial performance degradation around 10% – 30% for (i) misspecification of the noise distribution and 15% – 50% for (ii) contamination by outliers in all metrics compared to the likelihood well-specified cases. For image restoration tasks, similar degradation is observed in Table 1. Qualitatively, artifacts become evident, e.g., bright spots in deblurring results from IIGDM and PnPDM, as demonstrated in Figure 3, suggesting non-robustness to

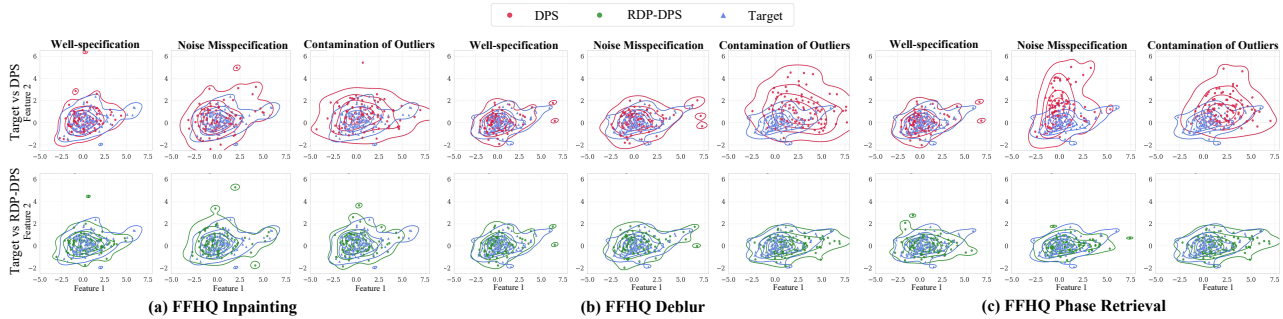


Figure 4. Posterior visualizations in Inception-v3 latent space. We compare recovered samples for (a) Inpainting, (b) Deblur, and (c) Phase Retrieval across well-specified, misspecified, and outlier-contaminated settings. Top: Standard DPS (●); Bottom: RDP-DPS (●). Target is marked by (▲). The density contours are estimated by kernel density estimation.

outlier contamination.

(RDP IMPROVEMENT.) The integration of RDP substantially mitigates these issues, showing robustness to the likelihood misspecification. For the inverse scattering task, we observe improvements of roughly 5% – 29% for (i) misspecification of the noise distribution and 20% – 50% improvement for (ii) contamination of outliers over baselines across all evaluation metrics. From Table 1, consistent improvements are observed on FFHQ-D and -PR. Qualitatively, the bright-spot artifacts seen with IIGDM and PnPDM are eliminated in their robust variants empowered by the proposed RDP, as demonstrated in Figure 3,7. This is consistent with our theory and design, as RDP is expected to adaptively down-weight extreme residuals and bound the influence of spurious large noise. These advantages hold for other tasks: reconstructions consistently show fewer artifacts and lower NMAE/LPIPS scores (Figure 3,7). At the distributional level, using a visualization in the Inception-v3 latent space (Figure 4, middle/right columns), DPS samples deviate from the target distribution under misspecification, whereas RDP-DPS remains closer, consistent with the proposed robust guidance via adaptive weighting.

We note that our robust module improves more under (ii) outlier contamination than under (i) the misspecification of the noise distributions (heavy-tailed Student-t distributions considered in this work). This is because it is easier to detect large-magnitude outliers than inconspicuous heavy-tailed noise in the signal. However, RDP has demonstrated its superior performance in both scenarios of likelihood misspecification.

(3) Can RDP be generalized with respect to: (i) being integrated into with different diffusion samplers and (ii) being effective across different tasks?

Yes. Our method is formulated as a robust guidance term derived from generalized Bayes, making it agnostic to the underlying solver. Consequently, it functions as a modular

component that can be seamlessly integrated into different diffusion samplers. For (ii), we validate this generalizability across a broad spectrum of challenges, ranging from high-dimensional linear restoration tasks on natural images to nonlinear physical measurements in scientific imaging. As shown in Table 1, our approach is highly effective in both regimes: it preserves competitive reconstruction quality in well-specified Gaussian settings and, crucially, significantly outperforms baseline methods when the likelihood model is misspecified. This consistent performance is supported not only by our numerical metrics but also by the visual stability observed in the qualitative results across all tested tasks; See Figure 3 and 7.

## 5. Conclusion

We discussed and provided theoretical analyzes for the *stability* and *robustness* phenomena in Bayesian inverse problems with diffusion models as priors. Meanwhile, we introduced a unified plug-and-play approach, *robust diffusion posteriors*, which can be readily incorporated into the existing gradient-based diffusion sampling methods. It delivers theoretical guarantees for robustness even when observations deviate from the assumed likelihood model without losing the property of stability. Extensive experimental results validate our theoretical analysis and demonstrate the effectiveness and robustness of the proposed method.

**Limitation and Future Work.** Our experiments primarily consider isotropic noise, whereas structured (e.g., correlated or spatially varying) noise is also common in practice. We provide a potential solution via an appropriate weighting function in the appendix, but a systematic evaluation is still needed. Empirically, our approach could be applied to discrete measurements, such as the Poisson distribution used for high-photon count signals. Extending the theoretical analysis to these cases requires additional effort and is left for future research.

## Impact Statement

This paper investigates the stability and robustness of diffusion priors in solving Bayesian inverse problems, proposing a modular approach that seamlessly integrates with a wide range of diffusion solvers. Our method is theoretically grounded and supported by comprehensive experimental validation. We do not identify any potential societal consequences that require specific discussion here.

## References

- Altamirano, M., Briol, F.-X., and Knoblauch, J. Robust and scalable bayesian online changepoint detection. In *International Conference on Machine Learning*, pp. 642–663. PMLR, 2023.
- Aravkin, A. Y., Burke, J. V., and Pillonetto, G. Robust and trend-following student’s t kalman smoothers. *SIAM Journal on Control and Optimization*, 52(5):2891–2916, 2014.
- Bao, F., Li, C., Sun, J., Zhu, J., and Zhang, B. Estimating the optimal covariance with imperfect mean in diffusion probabilistic models. In *International Conference on Machine Learning*, pp. 1555–1584. PMLR, 2022a.
- Bao, F., Li, C., Zhu, J., and Zhang, B. Analytic-dpm: an analytic estimate of the optimal reverse variance in diffusion probabilistic models. In *International Conference on Learning Representations*, 2022b.
- Boys, B., Girolami, M., Pidstrigach, J., Reich, S., Mosca, A., and Akyildiz, O. D. Tweedie moment projected diffusions for inverse problems. *Transactions on Machine Learning Research*, 2024.
- Cardoso, G. V., El Idrissi, Y. J., Le Corff, S., and Moulines, E. Monte carlo guided diffusion for bayesian linear inverse problems. In *International Conference on Learning Representations*, 2024.
- Chen, H., Ren, Y., Min, M. R., Ying, L., and Izzo, Z. Solving inverse problems via diffusion-based priors: An approximation-free ensemble sampling approach. *arXiv preprint arXiv:2506.03979*, 2025.
- Chung, H., Kim, J., McCann, M. T., Klasky, M. L., and Ye, J. C. Diffusion posterior sampling for general noisy inverse problems. In *International Conference on Learning Representations*, 2023.
- Daras, G., Chung, H., Lai, C.-H., Mitsufuji, Y., Ye, J. C., Milanfar, P., Dimakis, A. G., and Delbracio, M. A survey on diffusion models for inverse problems. *arXiv preprint arXiv:2410.00083*, 2024.
- De Vito, E., Rosasco, L., Caponnetto, A., De Giovannini, U., Odone, F., and Bartlett, P. Learning from examples as an inverse problem. *Journal of Machine Learning Research*, 6(5), 2005.
- Dou, Z. and Song, Y. Diffusion posterior sampling for linear inverse problem solving: A filtering perspective. In *The Twelfth International Conference on Learning Representations*, 2024.
- Douc, R. and Moulines, E. Limit theorems for weighted samples with applications to sequential monte carlo methods. *The Annals of Statistics*, pp. 2344–2376, 2008.
- Doucet, A., De Freitas, N., Gordon, N. J., et al. *Sequential Monte Carlo methods in practice*, volume 1. Springer, 2001.
- Duran-Martin, G., Altamirano, M., Shestopaloff, A. Y., Sánchez-Betancourt, L., Knoblauch, J., Jones, M., Briol, F.-X., and Murphy, K. Outlier-robust kalman filtering through generalised bayes. In *International Conference on Machine Learning*, pp. 12138–12171, 2024.
- Efron, B. Tweedie’s formula and selection bias. *Journal of the American Statistical Association*, 106(496):1602–1614, 2011.
- Graikos, A., Malkin, N., Jojic, N., and Samaras, D. Diffusion models as plug-and-play priors. *Advances in Neural Information Processing Systems*, 35:14715–14728, 2022.
- He, J., Hernández-Lobato, J. M., Du, Y., and Vargas, F. Rne: a plug-and-play framework for diffusion density estimation and inference-time control. *arXiv preprint arXiv:2506.05668*, 2025.
- Ho, J., Jain, A., and Abbeel, P. Denoising diffusion probabilistic models. *Advances in neural information processing systems*, 33:6840–6851, 2020.
- Ho, J., Salimans, T., Gritsenko, A., Chan, W., Norouzi, M., and Fleet, D. J. Video diffusion models. *Advances in neural information processing systems*, 35:8633–8646, 2022.
- Hosseini, B. and Nigam, N. Well-posed bayesian inverse problems: Priors with exponential tails. *SIAM/ASA Journal on Uncertainty Quantification*, 5(1):436–465, 2017.
- Huber, P. J. Robust statistics. In *International encyclopedia of statistical science*, pp. 1248–1251. Springer, 2011.
- Janati, Y., Moufad, B., Durmus, A., Moulines, E., and Olsson, J. Divide-and-conquer posterior sampling for denoising diffusion priors. *Advances in Neural Information Processing Systems*, 37:97408–97444, 2024.

- Janati, Y., Moulines, E., Olsson, J., and Oliviero-Durmus, A. Bridging diffusion posterior sampling and monte carlo methods: a survey. *Philosophical Transactions A*, 383 (2299):20240331, 2025.
- Janjić, T., Bormann, N., Bocquet, M., Carton, J., Cohn, S. E., Dance, S. L., Losa, S. N., Nichols, N. K., Potthast, R., Waller, J. A., et al. On the representation error in data assimilation. *Quarterly Journal of the Royal Meteorological Society*, 144(713):1257–1278, 2018.
- Karras, T., Aittala, M., Aila, T., and Laine, S. Elucidating the design space of diffusion-based generative models. *Advances in neural information processing systems*, 35: 26565–26577, 2022.
- Kawar, B., Elad, M., Ermon, S., and Song, J. Denoising diffusion restoration models. *Advances in neural information processing systems*, 35:23593–23606, 2022.
- Knapik, B. T., Van Der Vaart, A. W., and van Zanten, J. H. Bayesian inverse problems with gaussian priors. *The Annals of Statistics*, pp. 2626–2657, 2011.
- Knoblauch, J., Jewson, J., and Damoulas, T. An optimization-centric view on bayes’ rule: Reviewing and generalizing variational inference. *Journal of Machine Learning Research*, 23(132):1–109, 2022.
- Lu, C., Zheng, K., Bao, F., Chen, J., Li, C., and Zhu, J. Maximum likelihood training for score-based diffusion odes by high order denoising score matching. In *International conference on machine learning*, pp. 14429–14460. PMLR, 2022.
- Lu, C., Zhou, Y., Bao, F., Chen, J., Li, C., and Zhu, J. Dpm-solver++: Fast solver for guided sampling of diffusion probabilistic models. *Machine Intelligence Research*, pp. 1–22, 2025.
- Matsubara, T., Knoblauch, J., Briol, F.-X., and Oates, C. J. Robust generalised bayesian inference for intractable likelihoods. *Journal of the Royal Statistical Society Series B: Statistical Methodology*, 84(3):997–1022, 2022.
- Meng, C., Song, Y., Li, W., and Ermon, S. Estimating high order gradients of the data distribution by denoising. *Advances in Neural Information Processing Systems*, 34: 25359–25369, 2021.
- Moufad, B., Janati, Y., Bedin, L., Durmus, A. O., randal douc, Moulines, E., and Olsson, J. Variational diffusion posterior sampling with midpoint guidance. In *The Thirteenth International Conference on Learning Representations*, 2025. URL <https://openreview.net/forum?id=6EUtjXAvmj>.
- Ou, Z., Zhang, M., Zhang, A., Xiao, T. Z., Li, Y., and Barber, D. Improving probabilistic diffusion models with optimal diagonal covariance matching. In *International Conference on Learning Representations*, 2025.
- Rozet, F., Andry, G., Lanusse, F., and Louppe, G. Learning diffusion priors from observations by expectation maximization. *Advances in Neural Information Processing Systems*, 37:87647–87682, 2024.
- Sambridge, M. and Mosegaard, K. Monte carlo methods in geophysical inverse problems. *Reviews of Geophysics*, 40(3):3–1, 2002.
- Sohl-Dickstein, J., Weiss, E., Maheswaranathan, N., and Ganguli, S. Deep unsupervised learning using nonequilibrium thermodynamics. In *International Conference on Machine Learning*, pp. 2256–2265. pmlr, 2015.
- Song, J., Meng, C., and Ermon, S. Denoising diffusion implicit models. In *International Conference on Learning Representations*, 2021a.
- Song, J., Vahdat, A., Mardani, M., and Kautz, J. Pseudoinverse-guided diffusion models for inverse problems. In *International Conference on Learning Representations*, 2023a.
- Song, J., Zhang, Q., Yin, H., Mardani, M., Liu, M.-Y., Kautz, J., Chen, Y., and Vahdat, A. Loss-guided diffusion models for plug-and-play controllable generation. In *International Conference on Machine Learning*, pp. 32483–32498. PMLR, 2023b.
- Song, L. and Huang, H. Robust image restoration with an adaptive huber function based fidelity. *International Journal of Computer Vision*, 132(12):6127–6141, 2024.
- Song, Y. and Ermon, S. Generative modeling by estimating gradients of the data distribution. *Advances in Neural Information Processing Systems*, 32, 2019.
- Song, Y., Durkan, C., Murray, I., and Ermon, S. Maximum likelihood training of score-based diffusion models. *Advances in neural information processing systems*, 34: 1415–1428, 2021b.
- Song, Y., Shen, L., Xing, L., and Ermon, S. Solving inverse problems in medical imaging with score-based generative models. *arXiv preprint arXiv:2111.08005*, 2021c.
- Song, Y., Sohl-Dickstein, J., Kingma, D. P., Kumar, A., Ermon, S., and Poole, B. Score-based generative modeling through stochastic differential equations. In *International Conference on Learning Representations*, 2021d.
- Stein, C. M. Estimation of the mean of a multivariate normal distribution. *The Annals of Statistics*, pp. 1135–1151, 1981.

- Stuart, A. M. Inverse problems: a bayesian perspective. *Acta numerica*, 19:451–559, 2010.
- Sullivan, T. J. *Introduction to uncertainty quantification*, volume 63. Springer, 2015.
- Szegedy, C., Vanhoucke, V., Ioffe, S., Shlens, J., and Wojna, Z. Rethinking the inception architecture for computer vision. In *Proceedings of the IEEE conference on computer vision and pattern recognition*, pp. 2818–2826, 2016.
- Wang, Z., Bardsley, J. M., Solonen, A., Cui, T., and Marzouk, Y. M. Bayesian inverse problems with L1 priors: a randomize-then-optimize approach. *SIAM Journal on Scientific Computing*, 39(5):S140–S166, 2017.
- Wild, V. D., Ghalebikesabi, S., Sejdinovic, D., and Knoblauch, J. A rigorous link between deep ensembles and (variational) bayesian methods. *Advances in Neural Information Processing Systems*, 36:39782–39811, 2023.
- Wu, L., Trippe, B., Naesseth, C., Blei, D., and Cunningham, J. P. Practical and asymptotically exact conditional sampling in diffusion models. *Advances in Neural Information Processing Systems*, 36:31372–31403, 2023.
- Wu, Z., Sun, Y., Chen, Y., Zhang, B., Yue, Y., and Bouman, K. Principled probabilistic imaging using diffusion models as plug-and-play priors. *Advances in Neural Information Processing Systems*, 37:118389–118427, 2024.
- Zhang, M., Hawkins-Hooker, A., Paige, B., and Barber, D. Moment matching denoising gibbs sampling. *Advances in Neural Information Processing Systems*, 36:23590–23606, 2023.
- Zheng, H., Chu, W., Zhang, B., Wu, Z., Wang, A., Feng, B., Zou, C., Sun, Y., Kovachki, N. B., Ross, Z. E., Bouman, K., and Yue, Y. Inversebench: Benchmarking plug-and-play diffusion priors for inverse problems in physical sciences. In *International Conference on Learning Representations*, 2025.
- Zhu, Y., Zhang, K., Liang, J., Cao, J., Wen, B., Timofte, R., and Van Gool, L. Denoising diffusion models for plug-and-play image restoration. In *Proceedings of the IEEE/CVF conference on computer vision and pattern recognition*, pp. 1219–1229, 2023.

## A. Notation

Table 2. Summary of Key Notations.

Notation	Meaning
<i>Inverse Problem</i>	
$\mathbf{x}$	target variable
$\mathbf{y}_*$	noise-free measurement
$\mathbf{y}$	observed measurement
$\mathcal{F}(\cdot)$	Measurement model
$\epsilon$	Measurement noise ( $\mathbf{y} = \mathcal{F}(\mathbf{x}) + \epsilon$ )
<i>Diffusion Model</i>	
$p_{\text{data}}$	True data distribution
$\mathbf{x}_t$	Noised target variable at time $t \in [0, T]$
$\mathbf{x}_0$	Clean data samples
$\mathbf{s}_\theta(\mathbf{x}_t, t)$	Learned score function estimator
$\mathbf{x}_0(\mathbf{x}_t)$	Ideal denoised estimate using the true score $\nabla \log p_t$ ; $\mathbf{x}_{0 t} = \mathbb{E}[\mathbf{x}_0   \mathbf{x}_t]$
$\hat{\mathbf{x}}_0(\mathbf{x}_t)$	Predicted denoised estimate using the score network $\mathbf{s}_\theta$ ; approximation of $\mathbf{x}_{0 t}$
$\beta_t, \alpha_t$	Noise schedule and scaling factor
$p(\mathbf{x}_t   \mathbf{y})$	intermediate posterior distribution at time $t$
<i>Generalized Bayesian Inference</i>	
$\ell_{\mathbf{y}}(\mathbf{x}_t)$	Robust likelihood function
$\tau_t$	temperature (learning rate) at time $t$
$p^{(\ell)}(\mathbf{x}_t   \mathbf{y})$	Generalized posterior distribution at time $t$
$\hat{\mathbf{y}}_t$	Predicted observation; $\hat{\mathbf{y}}_t = \mathcal{F}(\hat{\mathbf{x}}_{0 t})$
$\mathbf{r}_t$	Residual vector; $\mathbf{r}_t = \mathbf{y} - \hat{\mathbf{y}}_t$
$\omega_t$	Learning rate/temperature at time $t$
$W(\mathbf{r}_t)$	Robust weighting matrix
PIF	Posterior Influence Function
<i>General Notation</i>	
$\mathbb{E}[\cdot]$	Expectation
$\mathbb{V}[\cdot]$	Variance (scalar) or Covariance matrix (vector)
$\nabla_{\mathbf{z}}$	Gradient with respect to $\mathbf{z}$
$\mathbf{I}$	Identity matrix
$\ \cdot\ _p$	$L_p$ norm
$J_f(\cdot)$	Jacobian of function $f$
$H_f(\cdot)$	Hessian of function $f$

## B. Review of Tweedie approximation in posterior sampling.

**Conditional Score Estimation: The *Plug-and-Play* Approach.** The most direct application of Tweedie’s approximation in posterior sampling is found in methods that attempt to estimate the conditional score  $\nabla_{\mathbf{x}_t} \log p(\mathbf{y}|\mathbf{x}_t)$  and plug it into the reverse SDE. This plug-and-play family, commonly referred to as Diffusion Posterior Sampling (DPS) (Graikos et al., 2022; Chung et al., 2023), replaces an intractable conditional expectation with a Tweedie-based point estimator. We focus our analysis on this class. Despite its empirical effectiveness, the approximation is heuristic and can induce systematic bias, as formalized in Theorem 3.4. To mitigate this approximation error, other methods utilize the structure of (linear) measurement model to derive more principled guidance signals. For instance, DDRM (Kawar et al., 2022) approaches linear inverse problems by performing diffusion in the spectral domain of the linear measurement model via SVD, while the IIGDM (Song et al., 2023a) employs the Moore-Penrose pseudoinverse to project the guidance signal directly onto the solution manifold consistent with the measurements. Moving beyond first-order point estimates, recent works incorporate second-order corrections. Rozet et al. (2024) propose matching the variance of  $p(\mathbf{x}_0|\mathbf{x}_t)$  by approximating it as a Gaussian rather than a Dirac delta. Similarly, Tweedie Moment Projected Diffusions (TMPD) (Boys et al., 2024) use higher-order Tweedie expansions to estimate the posterior covariance. Though statistically optimal for near-Gaussian distributions, this approach improves stability at the cost of computing the explicit Jacobian of the Tweedie estimator.

**Sequential Monte Carlo: Unbiased Estimator.** While the conditional score approach introduces systematic bias into the generation process due to Tweedie’s approximation, an alternative line of research utilizes Sequential Monte Carlo (SMC) to correct these errors (Wu et al., 2023; Janati et al., 2025). SMC methods, such as the Twisted Diffusion Sampler (TDS) (Wu et al., 2023) and Monte Carlo Guided Diffusion (MCGDiff) (Cardoso et al., 2024), provide theoretically well-founded algorithms for posterior sampling. Unlike the DPS, SMC offers strong guaranties: the weighted particle approximation is asymptotically exact as the number of particles goes to infinity (Doucet et al., 2001; Douc & Moulines, 2008). Recent work on the Radon-Nikodym Estimator (RNE) (He et al., 2025) has further unified these approaches. RNE demonstrates that the heuristic weight functions used in methods like TDS actually correspond to the theoretically optimal weights derived from the ratio of path measures between the forward and backward processes. This theoretical unification confirms that Tweedie’s approximation acts as the crucial link that makes these rigorous likelihood-ratio weights computable in practice. For linear inverse problems, Song et al. (2021c) introduces an auxiliary noise measurements sequence  $\{\mathbf{y}_t\}_t$  that is coupled to the latent diffusion trajectory  $\{\mathbf{x}_t\}_t$  through the same noise schedule. This coupling renders the intermediate likelihood  $p(\mathbf{y}_t|\mathbf{x}_t)$  linear Gaussian, yielding closed-form importance weights. This ensures that standard SMC updates remain tractable. Dou & Song (2024) further formalizes this approach within the Filtering for Posterior Sampling (FPS) framework. The resulting FPS-SMC algorithm provides a global consistency guarantee: as the number of particles approaches infinity, the approximation converges to the true Bayesian posterior. While SMC provides asymptotic guaranties, it suffers from the curse of dimensionality and requires a sufficient number of samples.

### C. Preliminaries of Tweedie’s Formula in Diffusion Models

**Proposition C.1** (First-order Tweedie Approximation (Chung et al., 2023)). *For the case of VP-SDE sampling,  $p(\mathbf{x}_0|\mathbf{x}_t)$  has the analytical posterior expectation, denoted as  $\mathbf{x}_{0|t}(\mathbf{x}_t) := \mathbb{E}[\mathbf{x}_0|\mathbf{x}_t]$ , is given by (Chung et al., 2023):*

$$\mathbf{x}_0(\mathbf{x}_t) = \frac{1}{\sqrt{\alpha(t)}} (\mathbf{x}_t + (1 - \alpha(t)) \nabla_{\mathbf{x}_t} \log p_t(\mathbf{x}_t)), \quad (5)$$

where  $\alpha(t) = \exp(-\int_0^t \beta(s) ds)$  is the accumulated noise variance.

By replacing the  $\nabla_{\mathbf{x}_t} \log p(\mathbf{x}_t)$  with the score network  $\mathbf{s}_\theta(\mathbf{x}_t, t)$ , the posterior expectation can be approximated as  $\hat{\mathbf{x}}_0 \approx \frac{1}{\sqrt{\alpha(t)}} (\mathbf{x}_t + (1 - \alpha(t)) \mathbf{s}_\theta(\mathbf{x}_t, t))$ .

**Proposition C.2** (Second-order Tweedie Approximation (Meng et al., 2021; Boys et al., 2024)). *For the case of VP-SDE, the conditional posterior  $p(\mathbf{x}_0 | \mathbf{x}_t)$  has an analytical posterior covariance given by:*

$$\mathbb{V}(\mathbf{x}_0|\mathbf{x}_t) = (1 - \alpha(t)) \left( \frac{1}{\alpha(t)} \mathbf{I} + \nabla_{\mathbf{x}_t}^2 \log p(\mathbf{x}_t) \right).$$

This follows from applying Tweedie’s formula to second-order moments. It introduces a curvature term to the first-order estimate, the Hessian of  $\log p(\mathbf{x}_t)$ —to capture posterior uncertainty. While the first-order formula gives the posterior mean  $\mathbb{E}(\mathbf{x}_0|\mathbf{x}_t)$ , the second-order formula gives the corresponding covariance  $\mathbb{V}(\mathbf{x}_0|\mathbf{x}_t)$ . Direct evaluation of  $\nabla_{\mathbf{x}_t}^2 \log p(\mathbf{x}_t)$  is often impractical because it requires second-order score information. In practice, this Hessian is approximated using the score network, either through automatic differentiation (Meng et al., 2021; Zhang et al., 2023; Boys et al., 2024) or by training an auxiliary network to estimate the Hessian term (Bao et al., 2022a;b; Ou et al., 2025).

*Remark C.3.* There is a straightforward algebraic relation between Proposition C.1 and C.2 such that

$$\mathbb{V}(\mathbf{x}_0|\mathbf{x}_t) = \sqrt{\alpha(t)} J_{\mathbf{x}_0}(\mathbf{x}_t) + \left( \frac{1 - 2\alpha(t)}{\alpha(t)} \right) \mathbf{I}, \quad (6)$$

where  $J_{\mathbf{x}_0}$  denotes the Jacobian of the posterior mean map. Note that this identity is not valid for an arbitrary Jacobian: the right-hand side need not be symmetric positive semidefinite and thus may fail to define a covariance matrix. It holds when  $J_T$  is the Jacobian of the *true* posterior-mean map induced by the associated density  $p(\mathbf{x}_t)$ .

**Proposition C.4** (Conditional Tweedie’s Formula). *Assuming a transition kernel  $p(\mathbf{x}_t|\mathbf{x}_0) = \mathcal{N}(\mathbf{x}_t; \sqrt{\alpha(t)}\mathbf{x}_0, (1 - \alpha(t))\mathbf{I})$  from VP-SDE, the score of the posterior marginal distribution at time  $t$  is exactly related to the conditional posterior expectation of  $\mathbf{x}_0$  by:*

$$\nabla_{\mathbf{x}_t} \log p(\mathbf{x}_t|\mathbf{y}) = - \frac{\mathbf{x}_t - \sqrt{\alpha(t)} \mathbb{E}[\mathbf{x}_0|\mathbf{x}_t, \mathbf{y}]}{1 - \alpha(t)}. \quad (7)$$

## D. Proof of main results

### D.1. Assumptions and Notations.

#### Notations.

- **Diffusion Process:** As stated in Section 2.2, we consider a VP-SDE with a noise schedule  $\beta(t)$  satisfying  $0 \leq \beta_{\min} \leq \beta(t) \leq \beta_{\max} < \infty$ . Defining  $\alpha(t) := \exp\left(-\int_0^t \beta(s) ds\right)$ , the transition kernel is  $p(\mathbf{x}_t | \mathbf{x}_0) = \mathcal{N}(\mathbf{x}_t; \sqrt{\alpha(t)}\mathbf{x}_0, (1 - \alpha(t))\mathbf{I})$ . Note that  $\alpha(t) \in [e^{-T\beta_{\max}}, 1]$ .
- $\|\cdot\|$ : Unless otherwise stated,  $\|\mathbf{x}\|$  denotes the Euclidean norm for vectors, and  $\|\mathbf{A}\| := \sup_{\|\mathbf{x}\|=1} \|\mathbf{A}\mathbf{x}\|$  denotes the operator norm for matrices or operators.
- In the following, we let  $\mathbf{x}_0(\mathbf{x}_t)$  denote the ideal denoised estimate computed using the true score function. We reserve  $\hat{\mathbf{x}}_0(\mathbf{x}_t)$  for the approximate estimate derived from the learned score network  $\mathbf{s}_\theta$ .

We introduce the following assumptions in more detail, commonly adopted in the theoretical analysis of DMs and BIPs, which will be used throughout the paper:

**Assumption D.1** (Measurement Model Regularity). The measurement model  $\mathcal{F}$  is Lipschitz smooth over  $\mathbb{R}^{d_x}$ . Specifically, there exist constants  $L_F, H_F > 0$  such that for all  $\mathbf{x}_1, \mathbf{x}_2 \in \mathbb{R}^{d_x}$ : (1)  $\|\mathcal{F}(\mathbf{x}_1) - \mathcal{F}(\mathbf{x}_2)\| \leq L_F \|\mathbf{x}_1 - \mathbf{x}_2\|$ , and (2)  $\|\nabla \mathcal{F}(\mathbf{x}_1) - \nabla \mathcal{F}(\mathbf{x}_2)\| \leq H_F \|\mathbf{x}_1 - \mathbf{x}_2\|$

**Assumption D.2** (Score Network Regularity). Suppose  $\mathbf{s}_\theta(\mathbf{x}_t, t)$  holds that  $\mathbf{s}_\theta(\mathbf{x}_t, t)$  is Lipschitz continuous with respect to  $\mathbf{x}$ , i.e., there exists a constant  $L_s > 0$  such that

$$\|\mathbf{s}_\theta(\mathbf{x}, t) - \mathbf{s}_\theta(\mathbf{x}', t)\| \leq L_s \|\mathbf{x} - \mathbf{x}'\|, \quad \forall \mathbf{x}, \mathbf{x}' \in \mathbb{R}^{d_x}, t \in [0, T].$$

**Assumption D.3** (Score Network Accuracy). The expected error of the score network is bounded:

$$\mathbb{E}[\|\nabla_{\mathbf{x}} \log p_t(\mathbf{x}) - \mathbf{s}_\theta(\mathbf{x}, t)\|_2^2] \leq \epsilon_s(t)^2, \quad \text{for any } t \in [0, T].$$

**Assumption D.4** (Compact support of clean targets). The clean target random variable  $\mathbf{x}_0$  is supported on a compact set  $\mathcal{X} \subset \mathbb{R}^{d_x}$ . In particular, there exists  $B_x < \infty$  such that  $\sup_{\mathbf{x} \in \mathcal{X}} \|\mathbf{x}\|_2 \leq B_x$ .

**Lemma D.5.** Suppose the measurement likelihood is Gaussian,  $p(\mathbf{y} | \mathbf{x}_0) = \mathcal{N}(\mathbf{y}; \mathcal{F}(\mathbf{x}_0), \sigma_y^2 \mathbf{I})$  with  $\sigma_y > 0$  at time  $t = 0$ . Under Assumption D.3, the expected estimation error of the unconditional score network, when evaluated under the conditional marginal distribution  $p_t(\mathbf{x}_t | \mathbf{y})$ , satisfies:

$$\mathbb{E}_{\mathbf{x}_t \sim p_t(\cdot | \mathbf{y})} \left[ \|\mathbf{s}_\theta(\mathbf{x}_t, t) - \nabla_{\mathbf{x}_t} \log p_t(\mathbf{x}_t)\|_2^2 \right] \leq \kappa_y \epsilon_s(t)^2,$$

where  $\kappa_y := p(\mathbf{y})^{-1} (2\pi\sigma_y^2)^{-d_y/2}$  is a finite constant for any observation  $\mathbf{y} \in \mathbb{R}^{d_y}$ .

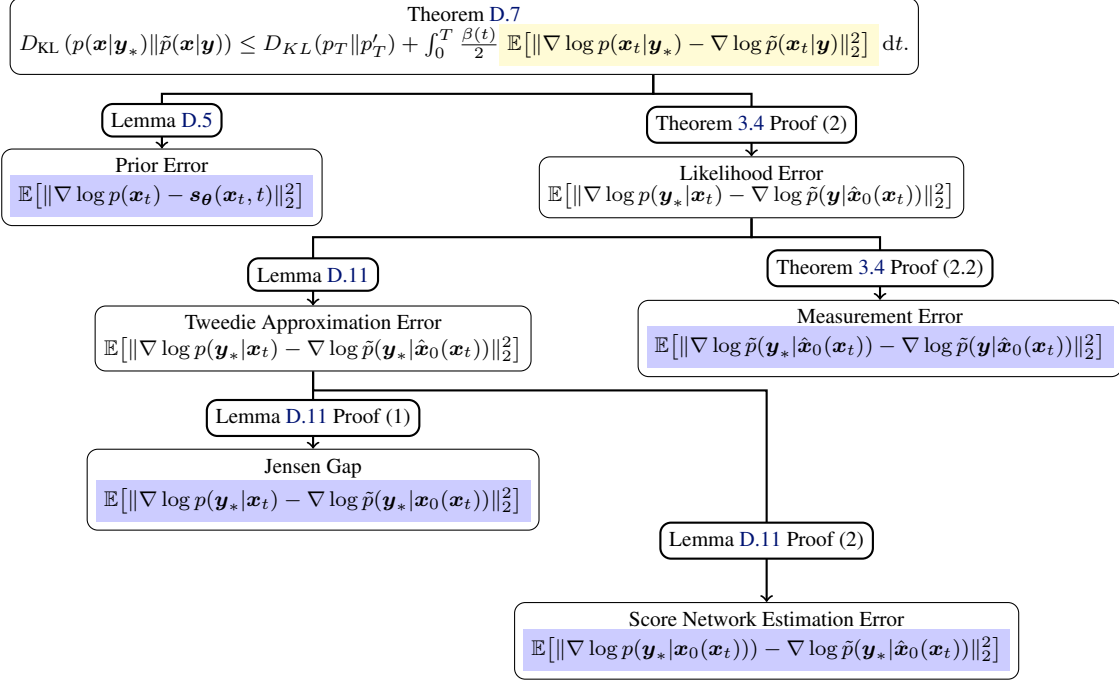
*Proof.* Let  $\mathcal{E}(\mathbf{x}_t) := \|\mathbf{s}_\theta(\mathbf{x}_t, t) - \nabla_{\mathbf{x}_t} \log p_t(\mathbf{x}_t)\|_2^2$  denote the squared error. We express the expectation under the conditional distribution:

$$\mathbb{E}_{\mathbf{x}_t \sim p_t(\cdot | \mathbf{y})} [\mathcal{E}(\mathbf{x}_t)] = \int \mathcal{E}(\mathbf{x}_t) \frac{p_t(\mathbf{x}_t | \mathbf{y})}{p_t(\mathbf{x}_t)} p_t(\mathbf{x}_t) d\mathbf{x}_t.$$

By Bayes' rule, the density ratio is  $\frac{p_t(\mathbf{x}_t | \mathbf{y})}{p_t(\mathbf{x}_t)} = \frac{p(\mathbf{y} | \mathbf{x}_t)}{p(\mathbf{y})}$ <sup>3</sup>. Since the likelihood  $p(\mathbf{y} | \mathbf{x}_t) = \mathbb{E}_{\mathbf{x}_0 | \mathbf{x}_t} [p(\mathbf{y} | \mathbf{x}_0)]$  is an expectation over Gaussian densities, it is uniformly bounded by the peak density  $M = (2\pi\sigma_y^2)^{-d_y/2}$ . Thus, the ratio is bounded by  $\kappa_y = M/p(\mathbf{y})$ . Substituting this into the integral:  $\mathbb{E}_{\mathbf{x}_t \sim p_t(\cdot | \mathbf{y})} [\mathcal{E}(\mathbf{x}_t)] \leq \kappa_y \int \mathcal{E}(\mathbf{x}_t) p_t(\mathbf{x}_t) d\mathbf{x}_t \leq \kappa_y \epsilon_s(t)^2$   $\square$

<sup>3</sup>Since the measurement model is Gaussian with  $\sigma_y > 0$ , the likelihood  $p(\mathbf{y} | \mathbf{x}_0)$  is strictly positive for all  $(\mathbf{x}_0, \mathbf{y})$ . Consequently, the marginal density  $p(\mathbf{y}) = \mathbb{E}_{\mathbf{x}_0} [p(\mathbf{y} | \mathbf{x}_0)]$  is strictly positive for all  $\mathbf{y} \in \mathbb{R}^{d_y}$ . Thus, the ratio is always well-defined and finite.

Figure 5. Overview of the proof of Theorem 3.4. The figure shows the decomposition of the integrand in the time integral from Girsanov theorem D.7 into interpretable error components, and indicates which assumptions, lemmas and intermediate steps are used to bound each term.



**Lemma D.6.** Suppose the likelihood  $p(\mathbf{y}|\mathbf{x})$  is a Gaussian distribution, such that  $p(\mathbf{y}|\mathbf{x}) = \mathcal{N}(\mathbf{y}; \mathcal{F}(\mathbf{x}), \sigma_y^2 \mathbf{I})$ . Under Assumption A1, the likelihood score  $\nabla_{\mathbf{x}} \log p(\mathbf{y}|\mathbf{x})$  is uniformly Lipschitz continuous with respect to the observation  $\mathbf{y}$ . Specifically, for any  $\mathbf{x} \in \mathcal{X}$ , we have:

$$\|\nabla_{\mathbf{x}} \log p(\mathbf{y}|\mathbf{x}) - \nabla_{\mathbf{x}} \log p(\mathbf{y}'|\mathbf{x})\| \leq L_{\text{ld}} \|\mathbf{y} - \mathbf{y}'\|, \quad \forall \mathbf{y}, \mathbf{y}' \in \mathbb{R}^{d_y},$$

where  $L_{\text{ld}} = L_F / \sigma_y^2$ .

*Proof.* The score of the Gaussian measurement model is given as  $\nabla_{\mathbf{x}} \log p(\mathbf{y}|\mathbf{x}) = \nabla \mathcal{F}(\mathbf{x})^\top \Sigma^{-1}(\mathbf{y} - \mathcal{F}(\mathbf{x}))$ , where  $\nabla \mathcal{F}(\mathbf{x})$  is the Jacobian of the measurement model. Denote  $\Delta_{\text{score}} = \nabla_{\mathbf{x}} \log p(\mathbf{y}|\mathbf{x}) - \nabla_{\mathbf{x}} \log p(\mathbf{y}'|\mathbf{x})$ , we have

$$\begin{aligned} \|\Delta_{\text{score}}\| &= \frac{1}{\sigma_y^2} \|\nabla \mathcal{F}(\mathbf{x})^\top (\mathbf{y} - \mathcal{F}(\mathbf{x})) - \nabla \mathcal{F}(\mathbf{x})^\top (\mathbf{y}' - \mathcal{F}(\mathbf{x}))\| \\ &= \frac{1}{\sigma_y^2} \|\nabla \mathcal{F}(\mathbf{x})^\top (\mathbf{y} - \mathbf{y}')\| \leq \underbrace{\frac{1}{\sigma_y^2} L_F}_{L_{\text{ld}}} \|\mathbf{y} - \mathbf{y}'\|, \end{aligned}$$

which concludes the proof.  $\square$

**Theorem D.7** (Girsanov Theorem). For any pair of diffusion processes  $\{\mathbf{x}_t\}_{t=0}^T$  and  $\{\mathbf{x}'_t\}_{t=0}^T$  on  $\mathbb{R}^{d_x}$  defined as follows:

$$\begin{aligned} d\mathbf{x} &= f(\mathbf{x}_t, t)dt + g(t)d\mathbf{w}_t \\ d\mathbf{x}' &= f'(\mathbf{x}'_t, t)dt + g(t)d\mathbf{w}'_t \end{aligned}$$

where  $f, f': \mathbb{R}^{d_x} \times [0, T] \rightarrow \mathbb{R}^{d_x}$  are the two drift functions and  $g: [0, T] \rightarrow \mathbb{R}_{>0}$  is the diffusion function. Let  $p_t$  and  $p'_t$  denote the distributions of  $\mathbf{x}_t$  and  $\mathbf{x}'_t$  for any  $t \in [0, T]$ ; then we have

$$D_{KL}(p_0 || p'_0) \leq D_{KL}(p_T || p'_T) + \int_0^T \frac{1}{2g(t)^2} \mathbb{E}[\|f(\mathbf{x}_t, t) - f'(\mathbf{x}_t, t)\|_2^2] dt. \quad (8)$$

*Proof.* The bound is a direct consequence of the Girsanov theorem, which relates the probability measures of diffusion processes under a change of drift. The result has been well established as standard in the analysis of generative diffusion models and is used to upper-bound the KL divergence between the true data distribution and the generated distribution by the time-accumulated mismatch between their respective score functions. For detailed derivations, we refer the reader to prior work, such as Theorem 1 in (Song et al., 2021b), Lemma 2.22 in (Wu et al., 2024), and Lemma C.1 in (Chen et al., 2025). A version adapted for the probability flow ODE formulation can be found in Theorem 3.1 of (Lu et al., 2022).

*Remark D.8.* In the VP-SDE, the reverse-time drift functions corresponding to the posterior  $p_t(\mathbf{x}_t|\mathbf{y})$  given the measurement  $\mathbf{y}$  are defined as:

$$f(\mathbf{x}_t, t) = -\beta(t) \left[ \frac{\mathbf{x}_t}{2} + \nabla \log p_t(\mathbf{x}_t|\mathbf{y}) \right].$$

Let  $f$  and  $\tilde{f}$  denote the target and approximate drift terms, respectively. Substituting the diffusion coefficient  $g(t) = \sqrt{\beta(t)}$ , the squared difference appearing in the Girsanov Theorem (Equation (8)) simplifies to:

$$\frac{1}{2g(t)^2} \mathbb{E} \left[ \|f(\mathbf{x}_t, t) - \tilde{f}(\mathbf{x}_t, t)\|^2 \right] = \frac{\beta(t)}{2} \mathbb{E}_{\mathbf{x}_t|\mathbf{y}} \left[ \|\nabla \log p_t(\mathbf{x}_t|\mathbf{y}) - \nabla \log \tilde{p}_t(\mathbf{x}_t|\mathbf{y})\|^2 \right].$$

In the following, we focus on analyzing the squared error term and establishing Theorems 3.4 and 3.5 via Theorem D.7.

## D.2. Proof of Theorem 3.4

**Lemma D.9.** *Assume the forward process (VP) is defined by the SDE  $d\mathbf{x}_t = -\frac{1}{2}\beta(t)\mathbf{x}_t dt + \sqrt{\beta(t)}d\mathbf{w}_t$  as in Section 2.2. The associated Gaussian perturbation kernel is given by  $\mathbf{x}_t|\mathbf{x}_0 \sim \mathcal{N}(\sqrt{\alpha(t)}\mathbf{x}_0, (1-\alpha(t))\mathbf{I})$ , where  $\alpha(t) = \exp\left(-\int_0^t \beta(s) ds\right)$ . Let  $\hat{\mathbf{x}}_0(\mathbf{x}_t)$  be the Tweedie estimator approximating the posterior mean  $\mathbb{E}[\mathbf{x}_0|\mathbf{x}_t]$  with the score network  $\mathbf{s}_\theta$ . Under Assumption A1 (Lipschitz continuity of the score network), the Jacobian of this estimator is bounded:  $\|J_{\hat{\mathbf{x}}_0}(\mathbf{x}_t)\| \leq L_{\hat{\mathbf{x}}_0}(t) < \infty$  for any time  $t \in [0, T]$ .*

*Proof.* The proof relies on Tweedie's formula, which relates the score of the marginal distribution to the posterior expectation. For the Gaussian perturbation kernel defined above and Proposition C.1, the Tweedie estimator is given as  $\hat{\mathbf{x}}_0(\mathbf{x}_t) = \frac{1}{\sqrt{\alpha(t)}}(\mathbf{x}_t + ((1-\alpha(t))\mathbf{s}_\theta(\mathbf{x}_t, t)))$ . We compute the Jacobian  $J_{\hat{\mathbf{x}}_0}(\mathbf{x}_t) = \nabla_{\mathbf{x}_t}\hat{\mathbf{x}}_0(\mathbf{x}_t)$  by differentiating with respect to  $\mathbf{x}_t$ ; then, for any time  $t \in [0, T]$ ,

$$\begin{aligned} \|J_{\hat{\mathbf{x}}_0}(\mathbf{x}_t)\| &= \left\| \frac{1}{\sqrt{\alpha(t)}} \left( \nabla_{\mathbf{x}_t}\mathbf{x}_t + (1-\alpha(t))\nabla_{\mathbf{x}_t}\mathbf{s}_\theta(\mathbf{x}_t, t) \right) \right\| \\ &= \frac{1}{\sqrt{\alpha(t)}} \left\| (I + (1-\alpha(t))\nabla_{\mathbf{x}_t}\mathbf{s}_\theta(\mathbf{x}_t, t)) \right\| \\ &\leq \frac{1}{\sqrt{\alpha(t)}} \left( \|I\| + (1-\alpha(t))\|\nabla_{\mathbf{x}_t}\mathbf{s}_\theta(\mathbf{x}_t, t)\| \right) \\ &\leq \frac{1}{\sqrt{\alpha(t)}} (1 + (1-\alpha(t))L_s) := L_{\hat{\mathbf{x}}_0}(t) < \infty. \end{aligned}$$

Since  $\alpha(t) \in [e^{-T\beta_{\max}}, 1]$ , the  $L_{\hat{\mathbf{x}}_0}(t)$  is finite for any time  $t \in [0, T]$ .  $\square$

**Lemma D.10.** *Consider the forward VP SDE defined as in Lemma D.9. Assume Assumptions A3 and A4 hold. Then, for any  $t \in [0, T]$ , there exists  $K(t) > 0$  such that  $\mathbb{E}\|\hat{\mathbf{x}}_{0|t}\|^2 \leq K(t) < \infty$ , where  $K(t) = \left( B_x + \frac{(1-\alpha(t))}{\sqrt{\alpha(t)}}\epsilon_s(t) \right)^2$ .*

*Proof.* With the target score function  $s_t(\mathbf{x}) = \nabla_{\mathbf{x}} \log p_t(\mathbf{x})$ , the exact posterior mean is given as  $\mathbf{x}_{0|t} = \frac{1}{\sqrt{\alpha(t)}}(\mathbf{x}_t + (1-\alpha(t))\nabla_{\mathbf{x}_t} \log p_t(\mathbf{x}_t))$ . The bound follows by taking the squared norm of the difference and then taking expectations;

$$\mathbb{E}\|\hat{\mathbf{x}}_{0|t} - \mathbf{x}_{0|t}\|^2 = \frac{(1-\alpha(t))^2}{\alpha(t)} \mathbb{E}\|\mathbf{s}_\theta(\mathbf{x}_t, t) - \nabla_{\mathbf{x}_t} \log p_t(\mathbf{x}_t)\|^2 \leq \frac{(1-\alpha(t))^2}{\alpha(t)} \epsilon_s(t)^2. \quad (9)$$

Finally, we have  $\mathbb{E}\|\hat{\mathbf{x}}_{0|t}\|^2 \leq \left( \sqrt{\mathbb{E}\|\mathbf{x}_{0|t}\|^2} + \sqrt{\frac{(1-\alpha(t))^2}{\alpha(t)}\epsilon_s(t)^2} \right)^2 \leq \left( B_x + \frac{(1-\alpha(t))}{\sqrt{\alpha(t)}}\epsilon_s(t) \right)^2 := K(t)$ .  $\square$

**Lemma D.11** (Bound on Tweedie Approximation Error). *Under Assumptions A1 and A3, given noise-free measurement  $\mathbf{y}_* = \mathcal{F}(\mathbf{x})$  the error between the true time-dependent likelihood score  $\nabla_{\mathbf{x}_t} \log p(\mathbf{y}_*|\mathbf{x}_t) = \nabla_{\mathbf{x}_t} \log \mathbb{E}_{\mathbf{x}_0|\mathbf{x}_t} [p(\mathbf{y}_*|\mathbf{x}_0)]$ , and the Tweedie-approximated score is bounded:*

$$\mathbb{E} [\|\nabla_{\mathbf{x}_t} \log p(\mathbf{y}_*|\mathbf{x}_t) - \nabla_{\mathbf{x}_t} \log \tilde{p}(\mathbf{y}_*|\hat{\mathbf{x}}_{0|t})\|^2] \leq \mathcal{E}_{\text{Tweedie}}(t) < \infty, \quad \text{for any time } t \in [0, T]$$

*Proof.* The error term in the expectation can be decomposed into two terms such as

$$\begin{aligned} \|\nabla_{\mathbf{x}_t} \log p(\mathbf{y}_*|\mathbf{x}_t) - \nabla_{\mathbf{x}_t} \log \tilde{p}(\mathbf{y}_*|\hat{\mathbf{x}}_{0|t})\|^2 &\leq \left( \underbrace{\|\nabla_{\mathbf{x}_t} \log p(\mathbf{y}_*|\mathbf{x}_t) - \nabla_{\mathbf{x}_t} \log p(\mathbf{y}_*|\mathbf{x}_{0|t})\|}_{\text{(1) Error from Jensen Gap}} \right. \\ &\quad \left. + \underbrace{\|\nabla_{\mathbf{x}_t} \log p(\mathbf{y}_*|\mathbf{x}_{0|t}) - \nabla_{\mathbf{x}_t} \log \tilde{p}(\mathbf{y}_*|\hat{\mathbf{x}}_{0|t})\|}_{\text{(2) Score Network Estimation}} \right)^2. \end{aligned}$$

$$\textbf{Term (1). } \|\nabla_{\mathbf{x}_t} \log p(\mathbf{y}_*|\mathbf{x}_t) - \nabla_{\mathbf{x}_t} \log p(\mathbf{y}_*|\mathbf{x}_{0|t})\| \leq \underbrace{\|\nabla_{\mathbf{x}_t} \log p(\mathbf{y}_*|\mathbf{x}_t)\|}_A + \underbrace{\|\nabla_{\mathbf{x}_t} \log p(\mathbf{y}_*|\mathbf{x}_{0|t})\|}_B.$$

With Proposition C.1 and C.4, the prior score and posterior score are given as  $\nabla_{\mathbf{x}_t} \log p(\mathbf{x}_t) = -\frac{\mathbf{x}_t - \alpha_t \mathbb{E}[\mathbf{x}_0|\mathbf{x}_t]}{\sigma_t^2}$  and  $\nabla_{\mathbf{x}_t} \log p(\mathbf{x}_t|\mathbf{y}_*) = -\frac{\mathbf{x}_t - \sqrt{\alpha(t)} \mathbb{E}[\mathbf{x}_0|\mathbf{x}_t, \mathbf{y}_*]}{1 - \alpha(t)}$  respectively. Then, with assumption D.4 (compact support of  $\mathbf{x}_0$ ), the term A can be bounded as

$$\|\nabla_{\mathbf{x}_t} \log p(\mathbf{y}_*|\mathbf{x}_t)\| = \left\| \frac{\sqrt{\alpha(t)}}{1 - \alpha(t)} (\mathbb{E}[\mathbf{x}_0|\mathbf{x}_t, \mathbf{y}_*] - \mathbb{E}[\mathbf{x}_0|\mathbf{x}_t]) \right\| \leq \frac{2\sqrt{\alpha(t)}}{1 - \alpha(t)} B_x$$

With Gaussian likelihood, the term B can be bounded as

$$\begin{aligned} \|\nabla_{\mathbf{x}_t} \log p(\mathbf{y}_*|\mathbf{x}_{0|t})\| &= \|J_{\mathbf{x}_0}(\mathbf{x}_t)^\top \nabla_{\mathbf{x}_{0|t}} \log p(\mathbf{y}_*|\mathbf{x}_{0|t})\| \\ &\leq \|J_{\mathbf{x}_0}(\mathbf{x}_t)\| \cdot \left\| \frac{J_F(\mathbf{x}_{0|t})}{\sigma_y^2} (\mathbf{y}_* - \mathcal{F}(\mathbf{x}_{0|t})) \right\| \\ &\leq \frac{1}{\sigma_y^2} L_{\mathbf{x}_0}(t) L_F \|\mathbf{y}_* - \mathcal{F}(\mathbf{x}_{0|t})\| \leq \frac{2}{\sigma_y^2} L_{\mathbf{x}_0}(t) L_F^2 B_x \end{aligned}$$

Then, the Term (1) can be bounded as  $\|\nabla_{\mathbf{x}_t} \log p(\mathbf{y}_*|\mathbf{x}_t) - \nabla_{\mathbf{x}_t} \log p(\mathbf{y}_*|\mathbf{x}_{0|t})\| \leq B_x \left( \frac{2}{\sigma_y^2} L_{\mathbf{x}_0}(t) L_F^2 + \frac{2\sqrt{\alpha(t)}}{1 - \alpha(t)} \right)$

**Term (2).** By the chain rule, Term (2) can be written and bounded as:

$$\begin{aligned} \mathbb{E} [\|\nabla_{\mathbf{x}_t} \log p(\mathbf{y}_*|\mathbf{x}_{0|t}) - \nabla_{\mathbf{x}_t} \log \tilde{p}(\mathbf{y}_*|\hat{\mathbf{x}}_{0|t})\|] &\leq \mathbb{E} [\|J_{\mathbf{x}_0}(\mathbf{x}_t)^\top \nabla \log p(\mathbf{y}_*|\mathbf{x}_{0|t})\|] + \mathbb{E} [\|J_{\hat{\mathbf{x}}_0}(\mathbf{x}_t)^\top \nabla \log p(\mathbf{y}_*|\hat{\mathbf{x}}_{0|t})\|] \\ &\leq \frac{L_F L_{\mathbf{x}_0}(t)}{\sigma_y^2} (\mathbb{E} [\|\mathbf{y}_* - \mathcal{F}(\mathbf{x}_{0|t})\|] + \mathbb{E} [\|\mathbf{y}_* - \mathcal{F}(\hat{\mathbf{x}}_{0|t})\|]) \\ &\leq \frac{L_F L_{\mathbf{x}_0}(t)}{\sigma_y^2} (2L_F B_x + L_F B_x + L_F \mathbb{E}[\|\hat{\mathbf{x}}_{0|t}\|]) \\ &\leq \frac{L_F^2 L_{\mathbf{x}_0}(t)}{\sigma_y^2} (3B_x + \sqrt{K(t)}) \end{aligned}$$

Combining the two terms, we get:

$$\begin{aligned} \mathbb{E} [\|\nabla_{\mathbf{x}_t} \log p(\mathbf{y}_*|\mathbf{x}_t) - \nabla_{\mathbf{x}_t} \log \tilde{p}(\mathbf{y}_*|\hat{\mathbf{x}}_{0|t})\|^2] &\leq B_x \left( \frac{2}{\sigma_y^2} L_{\mathbf{x}_0}(t) L_F^2 + \frac{2\sqrt{\alpha(t)}}{1 - \alpha(t)} \right) + \frac{L_F^2 L_{\mathbf{x}_0}(t)}{\sigma_y^2} (3B_x + \sqrt{K(t)}) \\ &:= \mathcal{E}_{\text{Tweedie}}(t) < \infty. \end{aligned}$$

□

**Lemma D.12** (Stability of Tweedie approximate posterior). *Let  $\tilde{p}(\mathbf{y}|\mathbf{x}_t) := p(\mathbf{y}|\hat{\mathbf{x}}_{0:t})$  be the Tweedie approximate likelihood defined in Section 2.2. Then, under mild assumptions on the forward model  $\mathcal{F}$  and the score network  $\mathbf{s}_\theta(\mathbf{x}_t, t)$ , the posterior map  $\mathbf{y} \mapsto \tilde{p}(\cdot | \mathbf{y})$  is Lipschitz continuous.*

**Proof.** By Theorem D.7, the KL divergence is bounded by the time integral of the expected squared difference between the reverse SDE drifts  $D_{KL}(\tilde{p}(\mathbf{x}_0|\mathbf{y})\|\tilde{p}(\mathbf{x}_0|\mathbf{y}')) \leq D_T + \int_0^T \frac{1}{2g(t)^2} \mathbb{E} \left[ \|\nabla_{\mathbf{x}_t} \log \tilde{p}_t(\mathbf{x}_t|\mathbf{y}) - \nabla_{\mathbf{x}_t} \log \tilde{p}_t(\mathbf{x}_t|\mathbf{y}')\|^2 \right] dt$ . We decompose the integral term as:

$$\begin{aligned} \nabla_{\mathbf{x}_t} \log \tilde{p}_t(\mathbf{x}_t|\mathbf{y}) - \nabla_{\mathbf{x}_t} \log \tilde{p}_t(\mathbf{x}_t|\mathbf{y}') &= \overline{\mathbf{s}_\theta(\mathbf{x}_t, t)} + \nabla_{\mathbf{x}_t} \log \tilde{p}_t(\mathbf{y}|\mathbf{x}_t) - \overline{\mathbf{s}_\theta(\mathbf{x}_t, t)} - \nabla_{\mathbf{x}_t} \log \tilde{p}_t(\mathbf{y}'|\mathbf{x}_t) \\ &= \nabla_{\mathbf{x}_t} \log \tilde{p}_t(\mathbf{y}|\mathbf{x}_t) - \nabla_{\mathbf{x}_t} \log \tilde{p}_t(\mathbf{y}'|\mathbf{x}_t). \end{aligned}$$

By the chain rule and Assumption A3,  $\nabla_{\mathbf{x}_t} \log \tilde{p}_t(\mathbf{x}_t|\mathbf{y}) = J_T(\mathbf{x}_t)^\top \nabla_{\hat{\mathbf{x}}_{0:t}} \log p(\mathbf{y} | \hat{\mathbf{x}}_{0:t})$ . Hence, using Lemma D.9, we have  $\|\nabla_{\mathbf{x}_t} \log \tilde{p}_t(\mathbf{x}_t|\mathbf{y}) - \nabla_{\mathbf{x}_t} \log \tilde{p}_t(\mathbf{x}_t|\mathbf{y}')\| \leq \|J_{\hat{\mathbf{x}}_0}(\mathbf{x}_t)\| L_{\text{lld}} \|\mathbf{y} - \mathbf{y}'\| \leq L_{\hat{\mathbf{x}}_0}(t) L_{\text{lld}} \|\mathbf{y} - \mathbf{y}'\|$ . Therefore,

$$D_{KL}(\tilde{p}(\cdot | \mathbf{y}) \|\tilde{p}(\cdot | \mathbf{y}')) \leq C_{\text{stable}} \|\mathbf{y} - \mathbf{y}'\|^2, \quad C_{\text{stable}} := \frac{L_{\text{lld}}^2 \beta_{\text{max}}}{2} \int_0^T L_{\hat{\mathbf{x}}_0}(t)^2 dt < \infty.$$

By Pinsker's inequality,  $\text{TV}(\tilde{p}(\cdot | \mathbf{y}), \tilde{p}(\cdot | \mathbf{y}')) \leq \sqrt{\frac{1}{2} D_{KL}} \leq \sqrt{\frac{1}{2} C_{\text{stable}}} \|\mathbf{y} - \mathbf{y}'\|$ , completing the proof.  $\square$

**Proof of Theorem 3.4.** By Theorem D.7, the KL divergence is bounded by the time integral of the expected squared difference between the reverse SDE drifts

$$D_{KL}(p(\mathbf{x}|\mathbf{y}_*)\|\tilde{p}(\mathbf{x}|\mathbf{y})) \leq D_T + \int_0^T \frac{1}{2g(t)^2} \mathbb{E} \left[ \|\nabla_{\mathbf{x}_t} \log p_t(\mathbf{x}_t|\mathbf{y}_*) - \nabla_{\mathbf{x}_t} \log \tilde{p}_t(\mathbf{x}_t|\mathbf{y})\|^2 \right] dt.$$

Denote  $M_t = \nabla_{\mathbf{x}_t} \log p_t(\mathbf{x}_t|\mathbf{y}_*) - \nabla_{\mathbf{x}_t} \log \tilde{p}_t(\mathbf{x}_t|\mathbf{y})$  as the drift mismatch between the approximated score and the true posterior score. The decomposition is as follows:

$$\begin{aligned} M_t &= (\nabla_{\mathbf{x}_t} \log p_t(\mathbf{x}_t) + \nabla_{\mathbf{x}_t} \log p_t(\mathbf{y}_*|\mathbf{x}_t)) - (\mathbf{s}_\theta(\mathbf{x}, t) + \nabla_{\mathbf{x}_t} \log \tilde{p}_t(\mathbf{y}|\hat{\mathbf{x}}_0(\mathbf{x}_t))) \\ &= \underbrace{(\nabla_{\mathbf{x}} \log p_t(\mathbf{x}) - \mathbf{s}_\theta(\mathbf{x}, t))}_{\text{Score Network Error}} + \underbrace{(\nabla_{\mathbf{x}_t} \log p_t(\mathbf{y}_*|\mathbf{x}_t) - \nabla_{\mathbf{x}_t} \log \tilde{p}_t(\mathbf{y}|\hat{\mathbf{x}}_0(\mathbf{x}_t)))}_{\mathcal{E}_t: \text{Likelihood Score Mismatch}}. \end{aligned}$$

(1) Bounding  $\mathbb{E}[\|\nabla_{\mathbf{x}} \log p_t(\mathbf{x}) - \mathbf{s}_\theta(\mathbf{x}, t)\|^2]$ . By Assumption A4 and Lemma ,  $\mathbb{E}[\|\nabla_{\mathbf{x}} \log p_t(\mathbf{x}) - \mathbf{s}_\theta(\mathbf{x}, t)\|^2] \leq \kappa_y \epsilon_s(t)^2$  for all  $t \in [0, T]$ .

(2) Bounding  $\mathbb{E}[\|\mathcal{E}_t\|^2]$ . By the triangle inequality, the likelihood score mismatch  $\mathcal{E}_t$  can be decomposed as:

$$\|\mathcal{E}_t\| \leq \underbrace{\|\nabla_{\mathbf{x}_t} \log p_t(\mathbf{y}_*|\mathbf{x}_t) - \nabla_{\mathbf{x}_t} \log \tilde{p}(\mathbf{y}_*|\hat{\mathbf{x}}_0(\mathbf{x}_t))\|}_{\mathcal{E}_{1,t}: \text{Tweedie Error}} + \underbrace{\|\nabla_{\mathbf{x}_t} \log \tilde{p}(\mathbf{y}_*|\hat{\mathbf{x}}_0(\mathbf{x}_t)) - \nabla_{\mathbf{x}_t} \log \tilde{p}(\mathbf{y}|\hat{\mathbf{x}}_0(\mathbf{x}_t))\|}_{\mathcal{E}_{2,t}: \text{Measurement Error}}.$$

Again,  $\mathbb{E}[\|\mathcal{E}_t\|^2] \leq 2\mathbb{E}[\|\mathcal{E}_{1,t}\|^2] + 2\mathbb{E}[\|\mathcal{E}_{2,t}\|^2]$ .

(2.1) Bounding  $\mathbb{E}[\|\mathcal{E}_{1,t}\|^2]$  (Tweedie Error). By Lemma D.11, we have  $\mathbb{E}[\|\mathcal{E}_{1,t}\|^2] \leq \mathcal{E}_{\text{Tweedie}}^2(t)$ .

(2.2) Bounding  $\mathbb{E}[\|\mathcal{E}_{2,t}\|^2]$  (Measurement Error). By the chain rule,

$$\begin{aligned} \|\mathcal{E}_{2,t}\| &= \|\nabla_{\mathbf{x}_t} \log \tilde{p}(\mathbf{y}_*|\hat{\mathbf{x}}_0(\mathbf{x}_t)) - \nabla_{\mathbf{x}_t} \log \tilde{p}(\mathbf{y}|\hat{\mathbf{x}}_0(\mathbf{x}_t))\| \\ &= \|J_{\hat{\mathbf{x}}_0}(\mathbf{x}_t)^\top \nabla_{\hat{\mathbf{x}}_{0:t}} \log \tilde{p}(\mathbf{y}_*|\hat{\mathbf{x}}_{0:t}) - J_{\hat{\mathbf{x}}_0}(\mathbf{x})^\top \nabla_{\hat{\mathbf{x}}_{0:t}} \log \tilde{p}(\mathbf{y}|\hat{\mathbf{x}}_{0:t})\| \\ &\leq \|J_{\hat{\mathbf{x}}_0}(\mathbf{x})\| \cdot \|\nabla_{\hat{\mathbf{x}}_{0:t}} \log \tilde{p}(\mathbf{y}_*|\hat{\mathbf{x}}_{0:t}) - \nabla_{\hat{\mathbf{x}}_{0:t}} \log \tilde{p}(\mathbf{y}|\hat{\mathbf{x}}_{0:t})\| \\ &\leq L_{\hat{\mathbf{x}}_0}(t) L_{\text{lld}} \|\mathbf{y}_* - \mathbf{y}\| = L_{\hat{\mathbf{x}}_0}(t) L_{\text{lld}} \|\epsilon\| \quad (\text{Lemma D.9 and Assumption A2}) \end{aligned}$$

Then, the second term is bounded by  $L_T^2 L_{\text{lld}}^2 \|\epsilon\|^2$ . Putting these bounds together,

$$\mathbb{E}[\|M_t\|^2] \leq 2\epsilon_s(t)^2 + 4\mathcal{E}_{\text{Tweedie}}^2(t) + 4L_T^2 L_{\text{lld}}^2 \|\epsilon\|^2.$$

Then, substituting into the time integral, we obtain the final result:

$$\begin{aligned}
 D_{KL}(p(\mathbf{x}_0|\mathbf{y})\|\tilde{p}(\mathbf{x}_0|\mathbf{y}')) &\leq D_T + \int_0^T \frac{1}{2g(t)^2} (2\epsilon_s(t)^2 + 4\mathcal{E}_{\text{Tweedie}}(t)^2 + 4L_T(t)^2 L_{\text{lld}}^2 \|\epsilon\|^2) dt \\
 &\leq D_T + \underbrace{\frac{\beta_{\max}}{2} \int_0^T \epsilon_s(t)^2 + 2\mathcal{E}_{\text{Tweedie}}(t)^2 dt}_{C_\theta} + \underbrace{\frac{\beta_{\max} L_{\text{lld}}^2}{2} \left( \int_0^T L_T(t)^2 dt \right)}_{C_{\text{stable in Lemma D.12}}} \|\epsilon\|^2 \\
 &\leq C_\theta + C_{\text{stable}} \|\epsilon\|^2
 \end{aligned}$$

Due to the properties established in the Lemma D.11 and D.9, the two integrals converge and  $C_\theta, C_{\text{stable}}$  are finite. The final bound confirms that the upper bound on the KL divergence grows quadratically with the perturbation size  $\|\epsilon\|$ , showing the stability of DPS and demonstrating that the error bound is radially unbounded.  $\square$

### D.3. Proof of Theorem 3.5 and Corollary 3.7

*Proof of Theorem 3.5.* Again by Girsanov Theorem D.7, we analyze the bound of the integrand

$$\|\nabla_{\mathbf{x}_t} \log p^{(\ell)}(\mathbf{x}_t|\mathbf{y}_*) - \nabla_{\mathbf{x}_t} \log p^{(\ell)}(\mathbf{x}_t|\mathbf{y})\| \leq \|\mathbf{s}_\theta(\mathbf{x}_t, t) - \mathbf{s}_\theta(\mathbf{x}_t, t)\| + \|\nabla_{\mathbf{x}_t} \log p^{(\ell)}(\mathbf{y}_*|\mathbf{x}_t) - \nabla_{\mathbf{x}_t} \log p^{(\ell)}(\mathbf{y}|\mathbf{x}_t)\|.$$

Then we take the square over the second term

$$\begin{aligned}
 \|\nabla_{\mathbf{x}_t} \log p^{(\ell)}(\mathbf{y}_*|\mathbf{x}_t) - \nabla_{\mathbf{x}_t} \log p^{(\ell)}(\mathbf{y}|\mathbf{x}_t)\|^2 &= \|J_T(\mathbf{x}_t) \left( \nabla_{\hat{\mathbf{x}}_{0|t}} \log p^{(\ell)}(\mathbf{y}_*|\hat{\mathbf{x}}_{0|t}) - \nabla_{\hat{\mathbf{x}}_{0|t}} \log p^{(\ell)}(\mathbf{y}|\hat{\mathbf{x}}_{0|t}) \right)\|^2 \\
 &\leq \|J_T(\mathbf{x}_t)\|^2 \|\nabla_{\hat{\mathbf{x}}_{0|t}} \log p^{(\ell)}(\mathbf{y}_*|\hat{\mathbf{x}}_{0|t}) - \nabla_{\hat{\mathbf{x}}_{0|t}} \log p^{(\ell)}(\mathbf{y}|\hat{\mathbf{x}}_{0|t})\|^2,
 \end{aligned} \tag{10}$$

where  $\|J_T(\mathbf{x}_t)\|^2 \leq L_T^2$  by Lemma D.11. We now show that the gradient of the loss  $\ell_{\mathbf{y}}$  is bounded. For a Gaussian measurement model  $p(\mathbf{y}|\mathbf{x})$ , up to constants,  $\ell_{\mathbf{y}}(\hat{\mathbf{x}}_{0|t}) = \sum_{i=1}^{d_y} \rho(r_i)$  with  $r_i = y_i - [\mathcal{F}(\hat{\mathbf{x}}_{0|t})]_i$  and  $\rho(r) = \frac{1}{2\sigma_y^2} w(r)r^2$ . Thus

$$\psi(r) := \rho'(r) = \frac{1}{2\sigma_y^2} (2r w(r) + r^2 w'(r)).$$

By the assumptions on  $w$ , for any  $r \in \mathbb{R}$ , we have  $|r w(r)| < \infty$  and  $|r^2 w'(r)| < \infty$ . Therefore, there exists a constant  $K$  such that  $\sup_{r \in \mathbb{R}_{\geq 0}} |\psi(r)| \leq K < \infty$ .

By Assumption 3.1,  $\|\nabla_{\hat{\mathbf{x}}_{0|t}} [\mathcal{F}(\hat{\mathbf{x}}_{0|t})]_i\| \leq L_F$ , so  $\|\nabla_{\mathbf{x}_t} \ell_{\mathbf{y}}(\mathbf{x}_{0|t})\| = \left\| \sum_{i=1}^{d_y} \psi(r_i) \nabla r_i \right\| \leq K L_F \sqrt{d_y}$ , uniformly over  $\mathbf{y}$ . Therefore,  $\|\nabla_{\hat{\mathbf{x}}_{0|t}} \ell_{\mathbf{y}_*} - \nabla_{\hat{\mathbf{x}}_{0|t}} \ell_{\mathbf{y}}\| \leq \|\nabla_{\hat{\mathbf{x}}_{0|t}} \ell_{\mathbf{y}_*}\| + \|\nabla_{\hat{\mathbf{x}}_{0|t}} \ell_{\mathbf{y}}\| \leq 2K L_F \sqrt{d_y}$ , and  $\|\nabla_{\mathbf{x}_t} \ell_{\mathbf{y}_*} - \nabla_{\mathbf{x}_t} \ell_{\mathbf{y}}\|^2 \leq 4 L_T^2(t) L_F^2 d_y K^2$  where  $C$  is finite and independent of  $\mathbf{y}$ . Taking into the time integral in Theorem D.7 and using the result in Lemma D.12, we get for any time  $t \in [0, T]$  and  $\mathbf{x} \in \mathcal{X}$

$$D_{KL} \left( p^{(\ell)}(\mathbf{x}_t|\mathbf{y}_*) \| p^{(\ell)}(\mathbf{x}_t|\mathbf{y}) \right) \leq \int_0^t \frac{4 L_T^2(t) L_F^2 d_y K^2}{\beta(\tau)^2} d\tau \leq 4 L_F^2 d_y K^2 \int_0^\tau \frac{L_T^2(t)}{\beta^2(\tau)} d\tau := C < \infty.$$

$\square$

*Proof of Corollary 3.7.* Following the proof sketch of Theorem 3.4, we analyze the expected squared difference between the posterior score functions of the respective reverse-time SDEs. Specifically, we compare: (1) The exact posterior score defined in Equation (2.2), where the likelihood score induced by the Gaussian measurement model  $\mathcal{N}(\mathcal{F}(\mathbf{x}_0), \sigma_y^2 \mathbf{I})$ ; and (2) the approximate robust posterior score, calculated using the learned score network and the robust DPS likelihood.

We decompose the difference  $\Delta_t = \nabla_{\mathbf{x}_t} \log p_t(\mathbf{x}_t|\mathbf{y}) - \nabla_{\mathbf{x}_t} \log p_t^{(\ell)}(\mathbf{x}_t|\mathbf{y})$  into three components:

$$\Delta_t = \underbrace{(\nabla_{\mathbf{x}_t} \log p_t(\mathbf{x}_t) - \mathbf{s}_\theta(\mathbf{x}_t, t))}_{\text{Prior Error } \mathcal{S}_t} + \underbrace{(\nabla_{\mathbf{x}_t} \log p(\mathbf{y}|\mathbf{x}) - \nabla_{\mathbf{x}_t} \log \tilde{p}(\mathbf{y}|\hat{\mathbf{x}}_0(\mathbf{x})))}_{\text{Tweedie Approx Error } \mathcal{E}_{\text{Tweedie}}(t)} + \underbrace{(\nabla_{\mathbf{x}} \log \tilde{p}(\mathbf{y}|\hat{\mathbf{x}}_0(\mathbf{x})) + \nabla_{\mathbf{x}} \ell_{\mathbf{y}}(\hat{\mathbf{x}}_0(\mathbf{x})))}_{\text{Bias } \mathcal{B}_t},$$

where the first term and second term have been shown bounded as  $C_\theta$  in Theorem 3.4. The third term,  $\mathcal{B}_t$ , quantifies the structural difference between the Gaussian likelihood gradient (high fidelity) and the robust loss gradient (outlier

suppression). Recall that for the Gaussian likelihood, the score is  $\nabla_{\mathbf{x}} \log p(\mathbf{y}|\mathbf{x}) = \frac{1}{\sigma_y^2} J_{\mathcal{F}}^\top \mathbf{r}$ . For the robust posterior, it is  $\nabla_{\mathbf{x}} \ell_{\mathbf{y}}(\mathbf{x}) = J_{\mathcal{F}}^\top \boldsymbol{\psi}(\mathbf{r})$ . Thus, the bias energy is:

$$\begin{aligned} \mathbb{E} [\|\mathcal{B}_t\|^2] &= \mathbb{E} \left[ \left\| J_{\hat{\mathbf{x}}_0}(\mathbf{x}_t) J_{\mathcal{F}}(\mathbf{x}_t)^\top \left( \frac{\mathbf{r}}{\sigma_y^2} - \boldsymbol{\psi}(\mathbf{r}) \right) \right\|^2 \right] \\ &\leq L_{\hat{\mathbf{x}}_0}^2(t) L_{\mathcal{F}}^2 \cdot \mathbb{E} \left[ \left\| \frac{\mathbf{r}}{\sigma_y^2} - \boldsymbol{\psi}(\mathbf{r}) \right\|^2 \right]. \end{aligned}$$

Using the IMQ weighting function, we derived the explicit form of the difference in the component-wise gradients:

$$\frac{r_i}{\sigma_y^2} - \psi(r_i) = \frac{r_i}{\sigma_y^2} - \frac{1}{\sigma_y^2} \frac{r_i + \frac{r_i^3}{2c^2}}{\left(1 + \frac{r_i^2}{c^2}\right)^{3/2}} = \frac{r_i}{\sigma_y^2} \left[ 1 - \frac{1 + \frac{r_i^2}{2c^2}}{\left(1 + \frac{r_i^2}{c^2}\right)^{3/2}} \right].$$

We analyze the asymptotic behavior of this term when  $c$  is large (the high-fidelity regime). Let  $u = r_i/c$ . The term in the brackets is  $1 - \frac{1+u^2/2}{(1+u^2)^{3/2}}$ . Using the Taylor expansion  $(1+u^2)^{-3/2} \approx 1 - \frac{3}{2}u^2 + O(u^4)$ , we have:

$$\frac{1 + \frac{u^2}{2}}{(1 + u^2)^{3/2}} \approx \left(1 + \frac{u^2}{2}\right) \left(1 - \frac{3u^2}{2}\right) \approx 1 - u^2 + O(u^4).$$

Substituting this back, the difference scales as  $\frac{r_i}{\sigma_y^2} [u^2] = \frac{r_i^3}{\sigma_y^2 c^2}$ . Consequently, the squared difference for the vector norm is bounded by:

$$\left\| \frac{\mathbf{r}}{\sigma_y^2} - \boldsymbol{\psi}(\mathbf{r}) \right\|^2 = \sum_{i=1}^{d_y} \left( \frac{r_i}{\sigma_y^2} \cdot O\left(\frac{r_i^2}{c^2}\right) \right)^2 \leq \frac{d_y R_{\max}^6}{\sigma_y^4 c^4},$$

where  $R_{\max} = 2L_F B_x$  is the bound on residuals derived from the compact support assumption.

Finally, substituting this into the time integral yields the bound for the bias term  $C_{\text{bias}}$ :

$$C_\ell = \int_0^T \frac{\beta(t)}{2} \mathbb{E} [\|\mathcal{B}_t\|^2] dt \leq \left( \frac{\beta_{\max} T L_T^2 L_{\mathcal{F}}^2 d_y R_{\max}^6}{2\sigma_y^4} \right) \cdot \frac{1}{c^4} = O(c^{-4}).$$

Thus,  $D_{KL}(p_t(\cdot|y_*) \| p_t^{(\ell)}(\cdot|y_*)) \leq C_\theta + O(c^{-4})$ . This confirms that as the robustness parameter  $c \rightarrow \infty$ , the robust posterior converges to the standard Bayesian posterior at a quartic rate.  $\square$

## E. Supplementary about RDP

### E.1. General Pseudo Algorithm

---

**Algorithm 2** RDP Plug in for Generic Diffusion Posterior Sampling
 

---

**Require:** observation  $\mathbf{y}$ , score network  $\mathbf{s}_\theta$ , noise schedule  $\{\beta_t\}_{t=0}^T$ , weight function  $w(\cdot)$ , temperature  $\{\tau_t\}_{t=0}^T$

- 1: Initialize  $\mathbf{x}_T \sim \mathcal{N}(\mathbf{0}, \mathbf{I})$
  - 2: **for**  $t = T, \dots, 1$  **do**
  - 3:    $\alpha_t = 1 - \beta_t$ ,    $\bar{\alpha}_t = \prod_{i=1}^t \alpha_i$
  - 4:    $\hat{\mathbf{x}}_{0|t} = \frac{1}{\sqrt{\bar{\alpha}_t}}(\mathbf{x}_t + (1 - \bar{\alpha}_t)\mathbf{s}_\theta(\mathbf{x}_t, t))$
  - 5:    $\hat{\mathbf{y}} = \mathcal{F}(\hat{\mathbf{x}}_{0|t})$  and  $\mathbf{r} = \mathbf{y} - \hat{\mathbf{y}}$
  - 6:    $\mathbf{W} = \text{diag}(w(r_1), \dots, w(r_m))$
  - 7:    $\ell_{\mathbf{y}}(\mathbf{x}_t) = \mathbf{W}^\top \log p(\mathbf{y} | \hat{\mathbf{x}}_0(\mathbf{x}_t))$
  - 8:    $\mathbf{x}_{t-1} = \text{UpdateStep}(\mathbf{x}_t, \mathbf{s}_\theta, \nabla \ell_{\mathbf{y}}(\mathbf{x}_t), \alpha_t, \beta_t)$
  - 9: **end for**
- 

- The likelihood term  $p(\mathbf{y} | \hat{\mathbf{x}}_0(\mathbf{x}_t))$  enforces data consistency; however, its specific formulation depends on the noise and operator assumptions. Our method can be used to *robustify* a broad family of algorithms. In this paper, we focus on the DPS algorithm, which approximates the likelihood via the surrogate mean  $\hat{\mathbf{x}}_{0|t}$  as a point estimate. For IIGDM (Song et al., 2023a) (which we use in our experiments), the method utilizes SVD to define the likelihood in the spectral domain, modeled as  $p(\mathbf{y} | \mathcal{F}(\hat{\mathbf{x}}_{0|t}), r_t \mathbf{I})$ . We integrate RDP by reweighting the log-likelihood objective:  $\ell_{\text{RDP}} \approx \mathbf{W}^\top \log \mathcal{N}(\mathbf{y} | \mathcal{F}(\hat{\mathbf{x}}_{0|t}), r_t \mathbf{I})$ , while additionally incorporating the annealing variance  $r_t$ . Furthermore, Boys et al. (2024) proposes a method for matching the variance using the second-order Tweedie’s formula. This higher-order approximation of variance can similarly be incorporated with RDP.
- The UPDATESTEP is solver-agnostic, allowing robust guidance to be integrated into various reverse-time discretizations. This includes standard SDE and ODE probability flow sampling, Predictor-Corrector (PC) schemes where Langevin dynamics refine the posterior estimate via  $\nabla \ell_{\mathbf{y}}$ , as well as recent progress in recent midpoint estimation approaches such as Janati et al. (2024); Moufad et al. (2025). Recent midpoint estimation such as Janati et al. (2024); Moufad et al. (2025), and Furthermore, the guidance term seamlessly extends to high-order solvers—such as DPM-Solver++ (Lu et al., 2025) or Heun’s method (Karras et al., 2022), enabling efficient sample generation with fewer steps.

### E.2. Other Weight functions

- **Mahalanobis-based.** When the measurement noise exhibits a nontrivial heterogeneous structure (e.g.,  $\sigma_i \neq \sigma_j$  for  $i \neq j$  in the Gaussian case), it is natural to measure residuals using Mahalanobis-based (MB) distance with a diagonal covariance  $\Sigma = (\sigma_1, \dots, \sigma_{d_y})$ , leading to weights  $w_i(y_i, \hat{y}_{t,i}) = (1 + \frac{(y_i - \hat{y}_{t,i})^2}{\sigma_i c^2})^{-\frac{1}{2}}$ .
- **Global scale.** Many diffusion samplers choose the step size based on the residual norm. For example, Chung et al. (2023) suggests choosing this step size to be inversely proportional to the measurement error norm  $\|\mathbf{y} - \mathcal{F}(\hat{\mathbf{x}}_0)\|_2$  (Daras et al., 2024). Within the GB framework, this corresponds to taking a global constant  $w = \frac{c}{\varepsilon + \|\mathbf{y} - \hat{\mathbf{y}}\|_2}$  for some constant  $c \in (0, 1]$  and a small  $\varepsilon > 0$ . This stabilizes the reverse process by preventing excessively large gradient steps. However, because it uses global scaling, it down-weights clean observations along with outliers and can thus be viewed as a special case of RDP.
- **Huber ( $L_1$  Loss).** Another well known robust loss function is Huberized Loss (Huber, 2011), which combines the sensitivity of squared error ( $L_2$ ) for small residuals with the robustness of absolute error ( $L_1$ ) for large residuals. For a residual  $r_i = y_i - \hat{y}_{t,i}$  and a specified transition threshold  $\delta$ , i.e.,

$$\ell_\delta(r) = \begin{cases} \frac{1}{2}r^2 & \text{if } |r| \leq \delta \\ \delta(|r| - \frac{1}{2}\delta) & \text{otherwise} \end{cases}$$

This effectively clips the gradients of outliers to a constant magnitude  $\delta$  as  $\delta(|r| - \frac{1}{2}\delta)$ , preventing large, corrupted measurements from dominating the guidance signal while preserving optimal Gaussian behavior for small errors.

## F. Additional Experiment Details

### F.1. Tasks

We evaluate our proposed method across a diverse set of inverse problems, ranging from standard linear image restoration tasks to complex nonlinear scientific imaging. The measurement process is generally modeled as  $\mathbf{y} = \mathcal{F}(\mathbf{x}) + \mathbf{n}$ , where  $\mathcal{F}(\cdot)$  represents the measurement model and  $\epsilon$  denotes the measurement noise.

- (Linear) Inverse Scattering: This task represents a linearized version of the general nonlinear inverse scattering problem. The measurement model is given by:  $\mathbf{y} = \mathbf{H}(\mathbf{u}_{\text{in}} \odot \mathbf{x}) + \epsilon$ , where  $\mathbf{u}_{\text{in}}$  is the known incident light field,  $\mathbf{H}$  is the Green’s function propagator, and  $\odot$  denotes the element-wise product. See more details in Section 3 of [Zheng et al. \(2025\)](#)
- Image Inpainting: The measurement model  $\mathcal{F}$  is a diagonal masking matrix  $\mathbf{M} \in \{0, 1\}^d$ , which effectively removes a random fraction of the pixels. The measurement is given by  $\mathbf{y} = \mathbf{M} \odot \mathbf{x} + \epsilon$ . The mask  $\mathbf{M}$  consists of a  $32 \times 32$  box placed at a random location within the image.
- (Gaussian) Deblurring: The measurement model  $\mathcal{F}$  corresponds to a convolution with an isotropic Gaussian kernel. The kernel is chosen with a standard deviation  $\sigma_{\text{blur}} = 3$  and a kernel size  $61 \times 61$ .
- Phase Retrieval: A critical problem in coherent diffractive imaging (e.g., X-ray crystallography), where detectors capture only the intensity of the diffracted wave. The measurement model is defined as  $\mathbf{y} = |\mathcal{T}(\mathbf{x})| + \mathbf{n}$ , where  $\mathcal{T}$  denotes the 2D discrete Fourier transform and  $|\cdot|$  is the element-wise magnitude operator. This problem is severely ill-posed due to the loss of phase information.

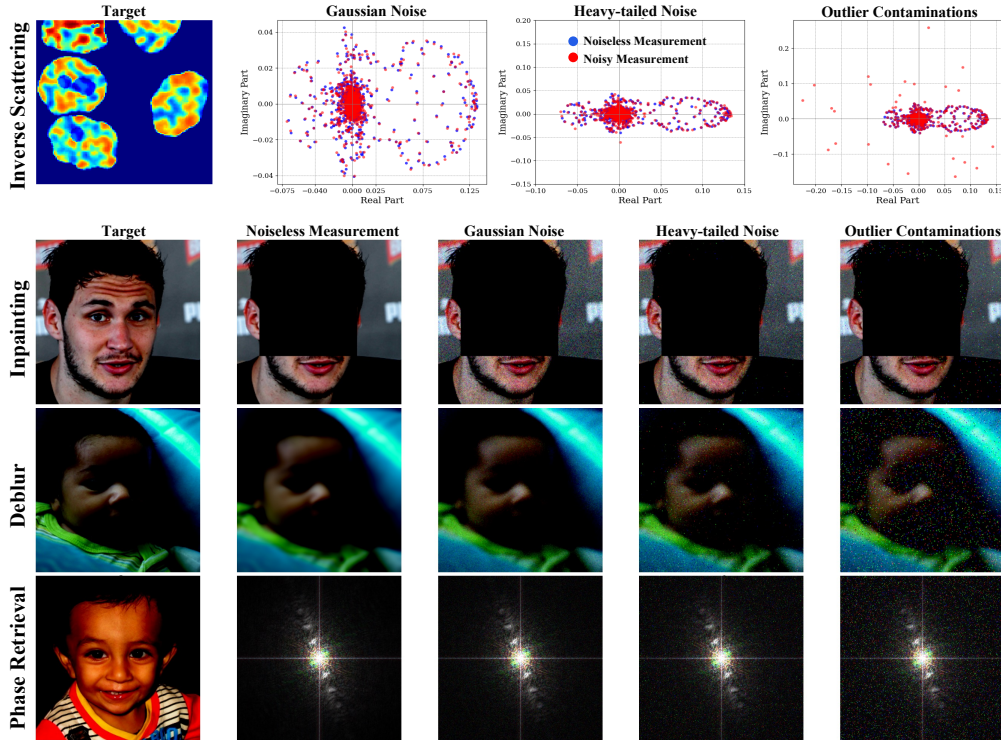


Figure 6. Visualization of measurements across three noise schemes (left→right: Gaussian, heavy-tailed, outlier).

## F.2. Experimental Design

In our numerical experiments in Section 4, we assess the robustness of the proposed modular approaches under three representative settings that commonly arise in scientific inverse problems:

- **Well-specified Likelihood (Gaussian Noise):** We utilize standard additive white Gaussian noise as the baseline control. This represents the ideal setting where the likelihood assumed by standard solvers matches the true noise distribution.
- **Distributional Misspecification (Heavy-tailed Noise):** To test robustness against violations of the Gaussian assumption, we model noise using a Student- $t$  distribution. The scale parameter is calibrated to match the standard deviation of the corresponding Gaussian baseline, while the degrees of freedom  $\nu$  control the tail heaviness. Heavy-tailed errors are extensively studied in robust estimation problems such as in Aravkin et al. (2014) and Janjić et al. (2018).
- **Outlier Contamination (Sparse Impulsive Noise):** We model corruption by replacing a fraction of the measurements with extreme, arbitrary values. The severity is controlled by two parameters: the corruption ratio  $p$  (the percentage of contaminated measurements) and the amplification factor  $m$  (the magnitude of the outlier values). This setting challenges the solver to identify and reject localized corruptions, simulating practical issues such as heat noise spikes or data transmission scattering errors. To simulate outlier corruptions, we first sample random noise from the base Gaussian distribution and then scale the magnitude of  $p\%$  of the total dimensions by a factor of  $m$ .

Table 3. Noise Schemes Summary. Well-specified lists the standard deviation  $\sigma_y$  used for Gaussian baselines. Misspecification details the Student- $t$  parameters ( $\nu$  and calibrated scale). Contamination specifies the outlier percentage ( $p$ ) and the magnitude factor ( $m$ ), where  $m$  denotes the multiplier of the signal’s peak dynamic range.

	Well-Specified ( $\mathcal{N}(0, \sigma_y^2)$ )	Misspecification (Student- $t$ )	Contamination (Outliers $p$ , Mag $m$ )
IS	$\sigma_y = 10^{-3}$	$\nu = 2.2$	$p = 1\%, m = 30\times$
FFHQ-I	$\sigma_y = 0.05$	$\nu = 2.5$	$p = 5\%, m = 30\times$
FFHQ-D	$\sigma_y = 0.05$	$\nu = 2.5$	$p = 5\%, m = 30\times$
FFHQ-PR	$\sigma_y = 10^{-3}$	$\nu = 2.5$	$p = 1\%, m = 10\times$

## F.3. Pretrained Diffusion Model Details

We use pretrained diffusion models with checkpoints provided by *InverseBench* (Zheng et al., 2025), which employ U-Net backbones, as in (Song et al., 2021d). Detailed configurations are listed in Table 4.

Table 4. Model network configurations for pre-trained diffusion models.

	Inverse Scattering	FFHQ
Input resolution	$128 \times 128$	$3 \times 256 \times 256$
# Attention blocks in encoder/decoder	5	6
# Residual blocks per resolution	1	3
Attention resolutions	16	16
# Parameters	26.8M	93.6M

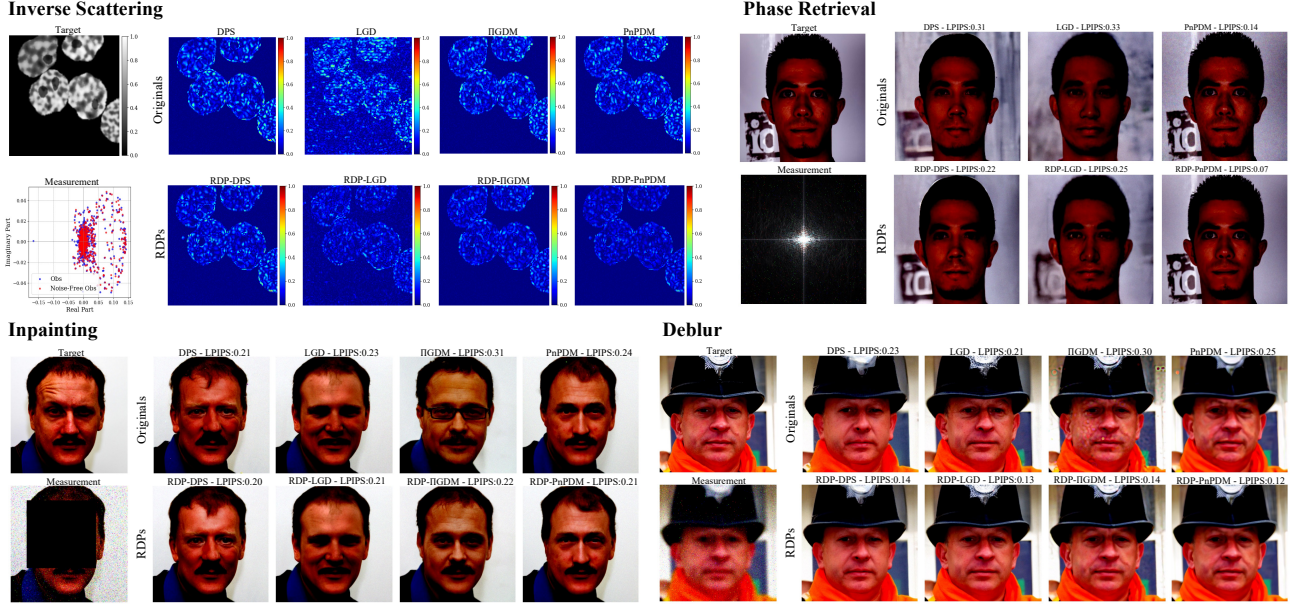


Figure 7. Qualitative results on all noise misspecification tasks: (a) Inverse Scattering, (b) Phase Retrieval, (c) Deblurring, and (d) Inpainting. In each panel, the leftmost column shows the ground truth and the contaminated observation. The remaining columns compare the original methods (top row) with their robustified versions using our sampler (bottom row); we report reconstruction absolute errors in (a) and reconstructed samples in (b)–(d).

Table 5. Hyperparameter tuning for different sampling methods and tasks. For other hyperparameters in PnPDM, we found it does not have significant effects to the results and we kept the configurations with (Zheng et al., 2025)

Method	Inverse Scattering		FFHQ-Inpaint		FFHQ-Deblur		FFHQ-PR	
	Used	Range	Used	Range	Used	Range	Used	Range
DPS								
Guidance Scale	350	[100, 500]	1	[0.1, 50]	5	[0.1, 50]	0.5	[0.1, 50]
LGD								
Guidance Scale	2500	[500, 5000]	1	[0.1, 50]	5	[0.1, 100]	1	[0.1, 100]
IGDM								
Stochasticity $\eta$	0.3	(0, 1]	0.95	(0, 1]	0.85	(0, 1]	-	-
PnPDM								
Annealing Max $\rho_{\max}$	20	[1, 100]	20	[1, 100]	10	[1, 100]	10	[1, 100]
Annealing decay rate $\rho$	0.9	[0.5, 1)	0.9	[0.5, 1)	0.9	[0.5, 1)	0.9	[0.5, 1)
Langevin step size $\tau$	$5 \times 10^{-4}$	(0, 1]	$5 \times 10^{-4}$	(0, 1]	$5 \times 10^{-4}$	(0, 1]	$1 \times 10^{-4}$	(0, 1]

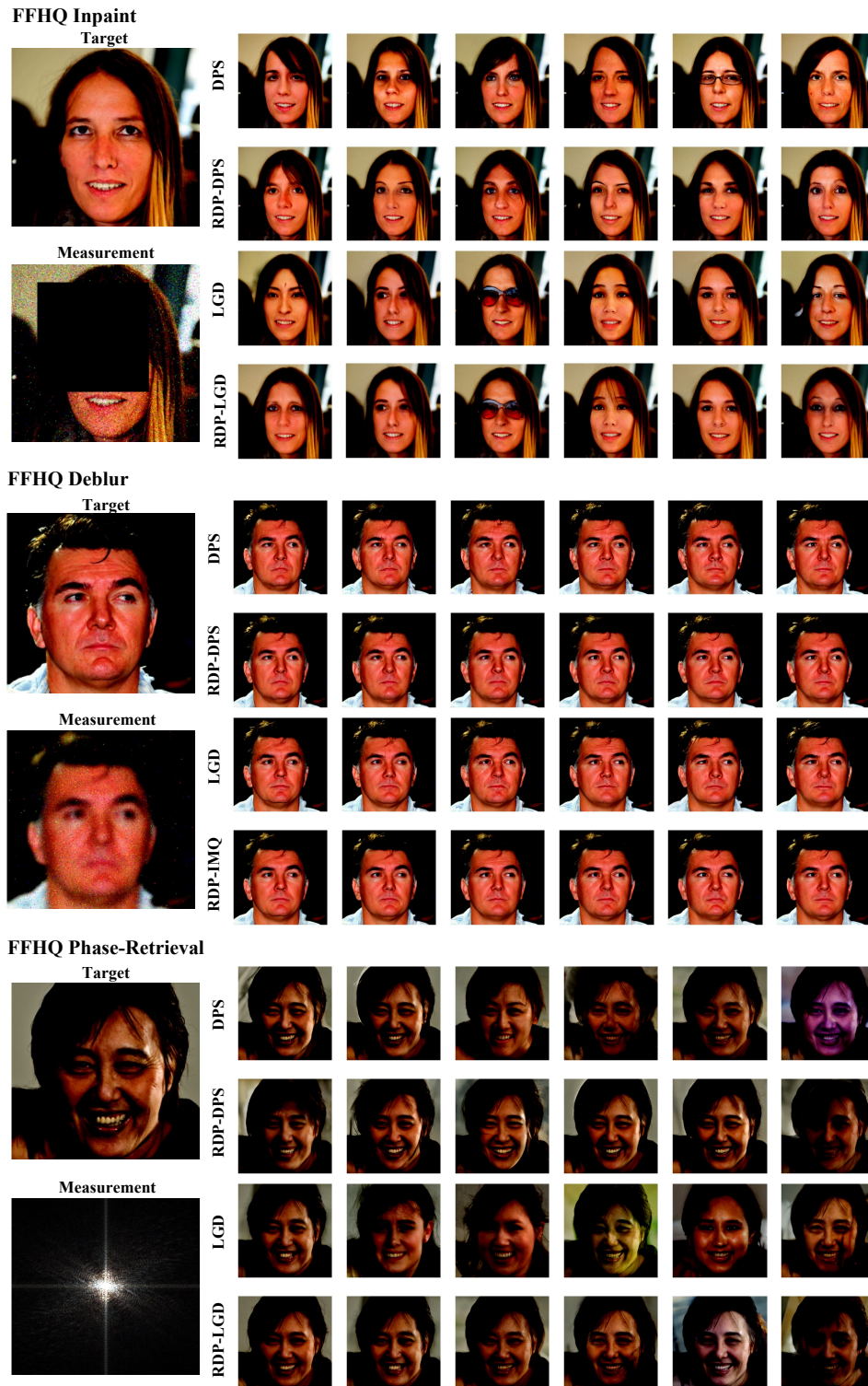


Figure 8. Multiple posterior samples from DPS and LGP with and without the RDPs on FFHQ, given heavy-tailed noises.

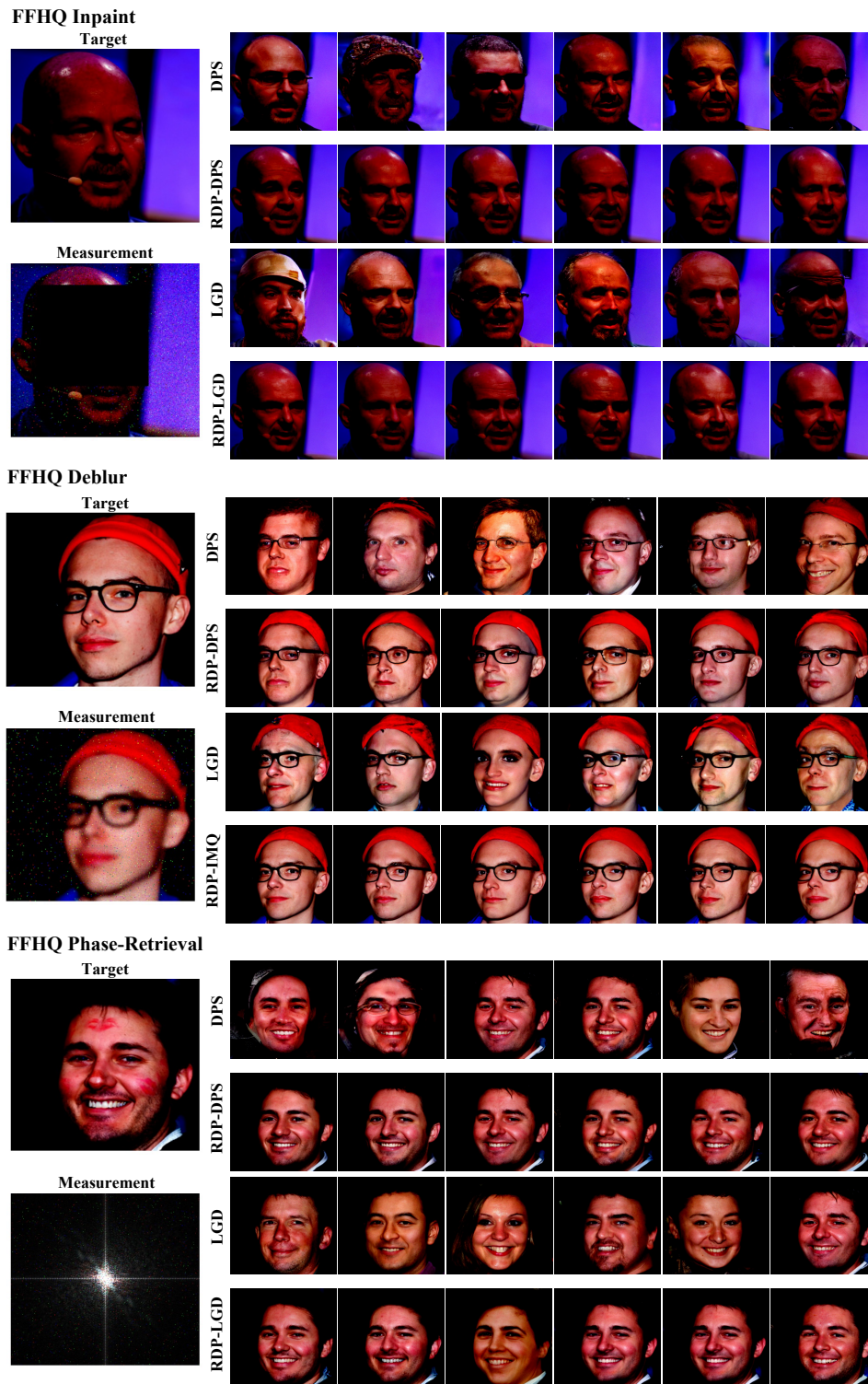


Figure 9. Multiple posterior samples from DPS and LGP with and without the RDPs on FFHQ, given observations corrupted by outliers.